# 1
# Electron Transfer Theories

## 1.1
## Introduction

Electron transfer (ET) is one of the most ubiquitous and fundamental phenomena in chemistry, physics, and biology [1–34]. Nonradiative and radiative ET are found to be a key elementary step in many important processes involving isolated molecules and supermolecules, ions and excess electrons in solution, condensed phase, surfaces and interfaces, electrochemical systems and biology, and in solar cells, in particular.

As a light microscopic particle, an electron easily tunnels through a potential barrier. Therefore, the process is governed by the general tunneling law formulated by Gamov [35]. The principal theoretical cornerstone for condensed phase ET was laid by Franck and Libby (1949–1952) who asserted that the Franck–Condon principle is applicable not only to the vertical radiative processes but also to nonradiative horizontal electron transfer. The next decisive step in the field was taken by Marcus and his colleagues [2, 17, 36] and Hash [37]. These authors articulated the need for readjustment of the coordination shells of reactants in self-exchange reactions and of the surrounding solvent to the electron transfer. They also showed that the electronic interaction of the reactants gives rise to the splitting at the intersection of the potential surfaces, which leads to a decrease in the energy barrier.

## 1.2
## Theoretical Models

### 1.2.1
### Basic Two States Models

#### 1.2.1.1 Landau–Zener Model

The nonadiabatic electron transfer between donor (D) and acceptor (A) centers is treated by the Fermi's golden rule (FGR) [38]

*Solar Energy Conversion. Chemical Aspects*, First Edition. Gertz Likhtenshtein.

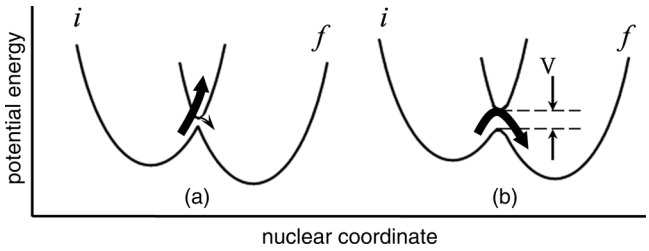


**Figure 1.1** Variation in the energy of the system along the reaction coordinate: (a) diabatic terms of the reactant (i) and products (f); (b) adiabatic terms of the ground state (f) and excited state (f). V is the resonance integral [9].

$$k_{ET} = \frac{2\pi V^2 FC}{h} \tag{1.1}$$

where FC is the Franck–Condon factor related to the probability of reaching the terms crossing area for account of nuclear motion and $V$ is an electronic coupling term (resonance integral) depending on the overlap of electronic wave functions in initial and final states of the process (see Figure 1.1).

At the transition of a system from one state to another, with a certain value of the coordinate $Q_{tr}$, the energy of the initial (i) and final (f) states of energy terms is the same and the law of energy conservation permits the term–term transition

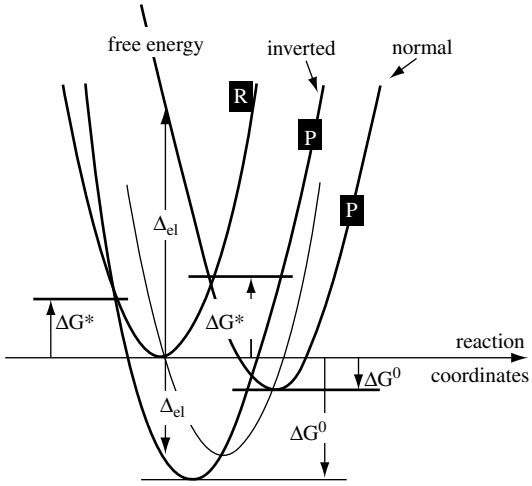


**Figure 1.2** Energy versus reaction coordinates for the reactants and the products for normal and inverted reactions, and the inversion curve. The electron in the initial state requires a positive excitation energy Δel for the normal reaction and a negative excitation energy - Δel for the inverted reaction (which could be directly emitted as light). There is a positive energy barrier $\Delta F^*$ in both cases between the reactants and the products that requires thermal activation for the reaction to occur. This energy barrier as well as the energy for a direct electron excitation vanishes for the inversion curve and then the electron transfer becomes ultrafast. Reproduced from Ref. [61].

(Figure 1.2). Generally, the rate constant of the transition in the crossing area is dependent on the height of the energetic barrier (activation energy, $E_a$), the frequency of reaching of the crossing area ($\psi$), and the transition coefficient ($\kappa$):

$$k_{tr} = \kappa\nu \exp(-E_a) \tag{1.2}$$

The transition coefficient $\kappa$ is related to the probability of the transition in the crossing area ($P$) and is described by the Landau–Zener equation [39, 40]:

$$\kappa = \frac{2P}{(1+P)} \tag{1.3}$$

where

$$P = 1 - \exp\left[\frac{-4\pi^2 V^2}{h\nu(S_i - S_f)}\right] \tag{1.4}$$

$V$ is the electronic coupling factor (the resonance integral), $\nu$ is the velocity of nuclear motion, and $S_i$ and $S_f$ are the slopes of the initial and final terms in the $Q_{tr}$ region. If the exponent of the exponential function is small, then

$$P = \frac{4\pi^2 V^2}{h\nu(S_i - S_f)} \tag{1.5}$$

and the process is nonadiabatic. Thus, the smaller the magnitude of the resonance integral $V$, the smaller is the probability of nonadiabatic transfer. The lower the velocity of nuclear motion and smaller the difference in the curvature of the terms, the smaller is the probability of nonadiabatic transfer. At $P = 1$, the process is adiabatic and treated by classical Arrhenius or Eyring equations.

The theory predicts a key role by electronic interaction, which is quantitatively characterized by the value of resonance integral $V$ in forming energetic barrier. If this value is sufficiently high, the terms are split with a decreasing activation barrier and the process occurs adiabatically. In another nonadiabatic extreme, where the interaction in the region of the coordinate $Q_{tr}$ is close to zero, the terms practically do not split, and the probability of transition i $\rightarrow$ f is very low.

#### 1.2.1.2 **Marcus Model**

According to the Marcus model [2, 3, 5, 17, 36], the distortion of the reactants, products, and solvent from their equilibrium configuration is described by identical parabolas, shifted relative to each other according to the driving force of the value of the process, standard Gibbs free energy $\Delta G_0$ (Figure 1.2). Within the adiabatic regime (strong electronic coupling, the resonance integral $V > 200\,\mathrm{cm}^{-1}$), in the frame of the Eyring theory of the transition state, the value of the electron transfer rate constant is

$$k_{ET} = \left(\frac{h\nu}{k_B T}\right) \exp - \left[\frac{(\lambda + \Delta G_0)^2}{4\lambda k_B T}\right] \tag{1.6}$$

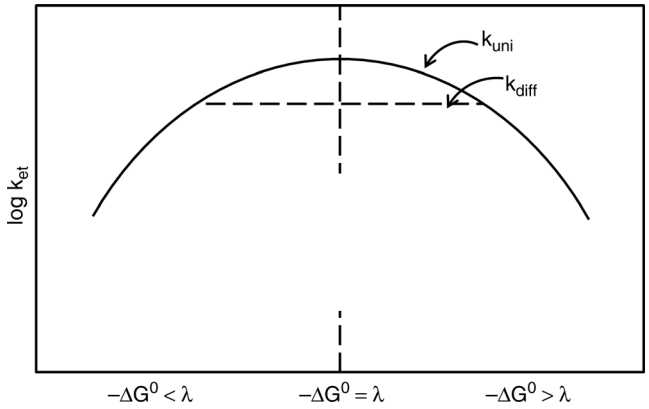


**Figure 1.3** Variation in the logarithm of the rate constant of electron transfer with the driving force for the reaction after Marcus [50].

where $\lambda$ is the reorganization energy defined as energy for the vertical electron transfer without replacement of the nuclear frame. Equation 1.6 predicts the log $k_{ET} - \Delta G_0$ relationships depending on the relative magnitudes of $\lambda$ and $\Delta G_0$ (Figure 1.3): (1) $\lambda > \Delta G_0$, when log $k$ increases if $\Delta G_0$ decreases (normal Marcus region); (2) $\lambda = \Delta G_0$, the reaction becomes barrierless; and (3) $\lambda < \Delta G_0$, when log $k$ decreases with increasing driving force.

The basic Marcus equation is valid in following conditions:

1) All reactive nuclear modes, that is, local nuclear modes, solvent inertial polarization modes, and some other kinds of collective modes, are purely classical. The electronic transition in the ET process is via the minimum energy at the crossing of the initial and final state potential surfaces.
2) The potential surfaces are essentially diabatic surfaces with insignificant splitting at the crossing and of parabolic shape. The latter reflects harmonic molecular motion with equilibrium nuclear coordinate displacement and a linear environmental medium response.
3) The vibrational frequencies and the normal modes are the same in the initial and final states.

The Marcus theory also predicts the Brönsted slope magnitude in the normal Marcus region:

$$\alpha_B = \frac{d\Delta G^{\#}}{d\Delta G_0} = \frac{1}{2}\left(1 + \frac{\Delta G_0}{\lambda}\right) \tag{1.7}$$

The processes driving force ($\Delta G_0$) can be measured experimentally or calculated theoretically. For example, when solvation after the process of producing photoinitiated charge pairing is rapid, $\Delta G_0$ can be approximately estimated by the following equation:

$$\Delta G_0 = E_{D/D^+} - (E_{A/A^+} + E_{D^*}) - \frac{e^2}{\varepsilon}(r_{D^+} + r_{A^-}) \tag{1.8}$$

where $E_{D/D^+}$ and $E_{A^+/A}$ are the standard redox potential of the donor and acceptor, respectively, $E_{D^*}$ is the energy of the donor exited state, $r_{D^+}$ and $r_{A^-}$ are the radii of the donor and acceptor, respectively, and $\varepsilon$ is the medium dielectric constant.

The values of $\lambda$ can be roughly estimated within the framework of a simplified model suggesting electrostatic interactions of oxidized donor ($D^+$) and reduced acceptor ($A^-$) of radii $r_{D^+}$ and $r_{A^-}$ separated by the distance $R_{DA}$ with media of dielectric constant $e_0$ and refraction index $n$:

$$\lambda = \frac{e^2}{2}\left(\frac{1}{n^2} - \frac{1}{e_0}\right)\left(\frac{1}{r_{D^+}} + \frac{1}{r_{A^-}} - \frac{2}{R_{DA}}\right) \tag{1.9}$$

#### 1.2.1.3 Electronic and Nuclear Quantum Mechanical Effects

The nonadiabatic electron transfer between donor (D) and acceptor (A) centers is treated by the FGR (Equation 1.1). The theory of nonadiabatic electron transfer was developed by Levich, Dogonadze, and Kuznetsov [41–43]. These authors, utilizing the Landau–Zener theory for the intersection area crossing suggesting harmonic one-dimensional potential surface, proposed a formula for nonadiabatic ET energy:

$$k_{ET} = \frac{2\pi V^2}{h\sqrt{4\pi\lambda k_B T}} \exp\left[-\frac{(\lambda + \Delta G_0)^2}{4\lambda k_B T}\right] \tag{1.10}$$

Therefore, the maximum rate of ET at $\lambda = \Delta G_0$ is given by

$$k_{ET\,(max)} = \frac{2\pi V^2}{h\sqrt{4\pi\lambda k_B T}} \tag{1.11}$$

Involvement of intramolecular high-frequency vibrational modes in electron transfer was considered [44–49]. For example, when the high-frequency mode ($h\nu$) is in the low-temperature limit and solvent dynamic behavior can be treated classically [1], the rate constant for nonadiabatic ET in the case of parabolic terms is given by

$$k_{ET} = \frac{\sum_j 2\pi F_j V^2}{h\lambda k_B T} \exp\left[-\frac{(jh\nu + \lambda_s + \Delta G_0)^2}{4\lambda k_B T}\right] \tag{1.12}$$

where $j$ is the number of high-frequency modes, $F_j = e^{-S}/j!$, $S = \lambda_v/h\psi$, and $\lambda_v$ and $\lambda_s$ denote the reorganization inside the molecule and solvent, respectively.

In the case of thermal excitation of the local molecular and medium high-frequency modes, theories mentioned before predicted the classical Marcus relation in the normal Marcus region. While in the inverted region, significant deviation on the parabolic energy gap dependence is expected (Figure 1.4). The inverted Marcus region cannot be experimentally observed if the stabilization of the first electron transfer product for the accounting of the high-frequency vibrational mode occurs faster than the equilibrium of the solvent polarization with the momentary charge distribution can be established. Another source of the deviation is the nonparabolic shape of the activation barrier [1].

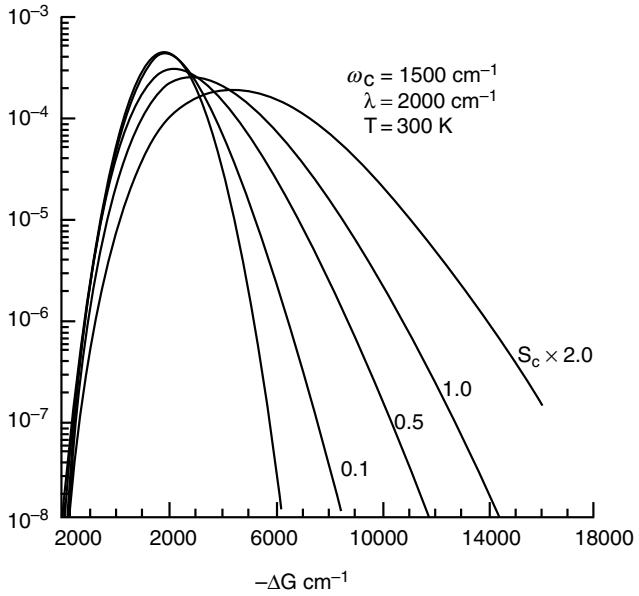


**Figure 1.4** The energy gap dependence of the nuclear Franck–Condon factor, which incorporates the role of the high-frequency intramolecular modes. $S_c = \Delta/2$ is the dimensionless electron–vibration coupling, given in terms that reduce replacement ($\Delta$) between the minimum of the nuclear potential surfaces of the initial and final electronic states [1]. Reproduced with permission.

A nonthermal electron transfer assisted by an intramolecular high-frequency vibrational mode has been theoretically investigated [18]. An analytical expression for the nonthermal transition probability in the framework of the stochastic point transition approach has been derived. For the strong electron transfer, the decay of the product state can vastly enhance the nonthermal transition probability in the whole range of parameters except for the areas where the probability is already close to unity. If the initial ion state is formed either by forward electron transfer or by photoexcitation, it may be visualized as a wave packet placed on the ion free energy term above the ion and the ground-state terms intersection (see Figure 6.1).

The Marcus inverted region cannot be observed experimentally when term-to-term transition in the crossing region is not a limiting step of the process as a whole (Figure 1.3) [50]. When ET reaction is very fast in the region of maximum rate, the process can be controlled by diffusion and, therefore, is not dependent on $\lambda$, $V^2$, and $\Delta G_0$. The integral encounter theory (IET) has been extended to the reactions limited by diffusion along the reaction coordinate to the level crossing points where either thermal or hot electron transfer occurs [18]. IET described the bimolecular ionization of the instantaneously excited electron donor $D^*$ followed by the hot geminate backward transfer that precedes the ion pair equilibration

$$D^* + A \underset{w_{21}}{\overset{w_{12}}{\longleftrightarrow}} [D^+ \quad \cdots \quad A^-] \xrightarrow{\bar{\varphi}} D^+ + A^-$$
$$w_{32} \updownarrow w_{23}$$
$$DA$$

and its subsequent thermal recombination tunneling is strong. It was demonstrated that the fraction of ion pairs that avoids the hot recombination is much smaller than their initial number when the electron tunneling is strong. The kinetics of recombination/dissociation of photogenerated radical pairs (RPs) was described with a generalized model (GM), which combines exponential models (EMs) and contact models (CMs) of cage effect dynamics [31]. Kinetics of nonthermal electron transfer controlled by the dynamical solvent effect was discussed in Ref. [11]. Recombination of ion pairs created by photoexcitation of viologen complexes is studied by a theory accounting for diffusion along the reaction coordinate to the crossing points of the electronic terms. The kinetics of recombination convoluted with the instrument response function were shown to differ qualitatively from the simplest exponential decay in both the normal and the inverted Marcus regions. The deviations of the exponentiality are minimal only in the case of activationless recombination and are reduced even more by taking into consideration a single quantum mode assisting the electron transfer

### 1.2.2
### Further Developments in the Marcus Model

#### 1.2.2.1 Electron Coupling

Variational transition-state theory was used to compute the rate of nonadiabatic electron transfer for a model of two sets of shifted harmonic oscillators [51]. The relationship to the standard generalized Langevin equation model of electron transfer was established and provided a framework for the application of variational transition-state theory in simulation of electron transfer in a microscopic (nonlinear) bath. A self-consistent interpretation based on a hybrid theoretical analysis that includes *ab initio* quantum calculations of electronic couplings, molecular dynamics simulations of molecular geometries, and Poisson–Boltzmann computations of reorganization energies was offered [52]. The analysis allowed to estimate the following parameters of systems under investigation: (1) reorganization energies, (2) electronic couplings, (3) access to multiple conformations differing both in reorganization energy and in electronic coupling, and (4) donor–acceptor coupling dependence on tunneling energy, associated with destructively interfering electron and hole-mediated coupling pathways. Fundamental arguments and detailed computations show that the influence of donor spin state on long-range electronic interactions is relatively weak.

The capability of multilevel Redfield theory to describe ultrafast photoinduced electron transfer reactions and the self-consistent hybrid method was investigated [53]. Adopting a standard model of photoinduced electron transfer in a condensed phase environment, the authors considered electron transfer reactions in the normal and inverted regimes, as well as for different values of the electron transfer parameters, such as reorganization energy, electronic coupling, and temperature.

A semiclassical theory of electron transfer reactions in Condon approximation and beyond was developed in [54]. The effect of the modulation of the electronic wave functions by configurational fluctuations of the molecular environment on the kinetic parameters of electron transfer reactions was discussed. A new formula for the transition probability of nonadiabatic electron transfer reactions was obtained and regular method for the calculation of non-Condon corrections was suggested. Quantum Kramers-like theory of the electron transfer rate from weak-to-strong electronic coupling regions using Zhu–Nakamura nonadiabatic transition formulas was developed to treat the coupled electronic and nuclear quantum tunneling probability [55]. The quantum Kramers theory to electron transfer rate constants was generalized. The application in the strongly condensed phase manifested that the approach correctly bridges the gap between the nonadiabatic (Fermi's golden rule) and adiabatic (Kramers theory) limits in a unified way, and leads to good agreement with the quantum path integral data at low temperature.

In work [56], electron transfer coupling elements were extracted from constrained density functional theory (CDFT). This method made use of the CDFT energies and the Kohn–Sham wave functions for the diabatic states. A method of calculation of transfer integrals between molecular sites, which exploits few quantities derived from density functional theory electronic structure computations and does not require the knowledge of the exact transition state coordinate, was conceived and implemented [57]. The method used a complete multielectron scheme, thus including electronic relaxation effects. The computed electronic couplings can then be combined with estimations of the reorganization energy to evaluate electron transfer rates. On the basis of the generalized nonadiabatic transition-state theory [58], the authors of the work [59, 60] presented a new formula for electron transfer rate, which can cover the whole range from adiabatic to nonadiabatic regime in the absence of solvent dynamics control. The rate was expressed as a product of the Marcus theory and a coefficient that represents the effects of nonadiabatic transition at the crossing seam surface. The numerical comparisons were performed with different approaches and the present approach showed an agreement with the quantum mechanical numerical solutions from weak to strong electronic coupling.

A nonadiabatic theory for electron transfer and application to ultrafast catalytic reactions has been discussed in Ref. [61]. The author proposed a general formalism that not only extends those used for the standard theory of electron transfer but also becomes equivalent to it far from the inversion point. In the vicinity of the inversion point when the energy barrier for ET is small, the electronic frequencies become of the order of the phonon frequencies and the process of electron tunneling is nonadiabatic because it is strongly coupled to the phonons. It was found that when the model parameters are fine-tuned, ET between donor and acceptor becomes reversible and this system is a coherent electron–phonon oscillator (CEPO). The acceptor that does not capture the electron may play the role of a catalyst (Figure 1.5). Thus, when the catalyst is fine-tuned with the donor in order to form a CEPO, it may trigger an irreversible and ultrafast electron transfer (UFET) at low temperature between the donor and an extra acceptor. Such a trimer system may be regulated by small perturbations and behaves as a molecular transistor.

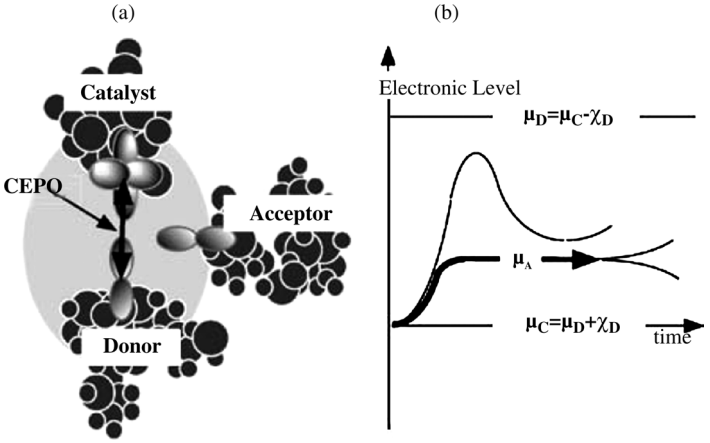


**Figure 1.5** Principle of ET with a coherent electron–phonon oscillator [61].

Two weakly coupled molecular units of donor and catalyst generate a CEPO. This system is weakly coupled to a third unit, the acceptor (Figure 1.5a). An electron initially on the donor generates an oscillation of the electronic level of the CEPO. If the bare electronic level of a third molecular unit (acceptor) is included in the interval of variation, as soon as resonance between the CEPO and the acceptor is reached, ET is triggered irreversibly to the acceptor (Figure 1.5b). The authors suggested that because of their ability to produce UFET, the concept of CEPOs could be an essential paradigm for understanding the physics of the complex machinery of living systems.

Perturbation molecular orbital (PMO) theory was used to estimate the electronic matrix element in the semiclassical expression for the rate of nonadiabatic electron transfer at ion–molecular collisions [62]. It was shown that the electron transfer efficiency comes from the calculated ET rate divided by the maximum calculated ET rate and by dividing the observed reaction rate by the collision rate, calculated by the PMO treatment of ion–molecular collision rates.

#### 1.2.2.2 **Driving Force and Reorganization Energy**

Several works were devoted to models for medium reorganization and donor–acceptor coupling [63–78]. The density functional theory based on *ab initio* molecular dynamics method combines electronic structure calculation and statistical mechanics and was used for first-principles computation of redox free energies at one-electron energy [66]. The authors showed that this is implemented in the framework of the Marcus theory of electron transfer, exploiting the separation in vertical ionization and reorganization contributions inherent in Marcus theory. Direct calculation of electron transfer parameters through constrained density functional theory was a subject of the work by Wu and Van Voorhis [67]. It was shown that constrained density functional theory can be used to access diabatic potential energy surfaces in the Marcus theory of electron transfer, thus providing a means to directly calculate the driving force and the inner sphere reorganization energy. The influence

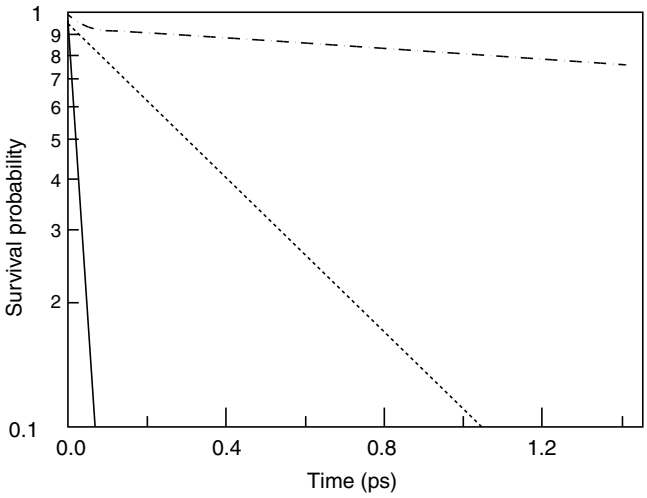


**Figure 1.6** Survival probability as a function of time for D-B-A systems containing three (solid line), four (dotted line), and five (dashed line) subunits. All curves were calculated for the D-B-A system with the energy gap $\Delta\varepsilon$ between the donor and the equienergetic bridge equal to 1.2 eV. The value of the charge transfer integral $V$ was taken to be equal to 0.3 eV [68].

of static and dynamic torsional disorder on the kinetics of charge transfer (CT) in donor–bridge–acceptor (D-B-A) systems has been investigated theoretically using a simple tight binding model [68]. Modeling of CT beyond the Condon approximation revealed two types of non-Condon (NC) effects. It was found that if $\tau_{rot}$ is much less than the characteristic time, $\tau_{CT}$, of CT in the absence of disorder, the NC effect is static and can be characterized by rate constant for the charge arrival on the acceptor. For larger $\tau_{rot}$, the NC effects become purely kinetic and the process of CT in the tunneling regime exhibits timescale invariance, the corresponding decay curves become dispersive, and the rate constant turns out to be time dependent. In the limit of very slow dynamic fluctuations, the NC effects in kinetics of CT were found to be very similar to the effects revealed for bridges with the static torsional disorder. The authors argued that experimental data reported in the literature for several D-B-A systems must be attributed to the multistep hopping mechanism of charge motion rather than to the mechanism of single-step tunneling. Survival probability as a function of time for D-B-A systems is shown in Figure 1.6.

The theory developed by Fletcher in Refs [71, 72] took into account the fact that charge fluctuations contribute to the activation of electron transfer, besides dielectric fluctuations. It was found that highly polar environments are able to catalyze the rates of thermally activated electron transfer processes because under certain well-defined conditions, they are able to stabilize the transient charges that develop on transition states. Plots of rate constant for electron transfer versus driving force are shown in Figure 1.7, which is drawn on the assumption that electron transfer is nonadiabatic and proceeds according to Dirac's time-dependent perturbation theory. On the

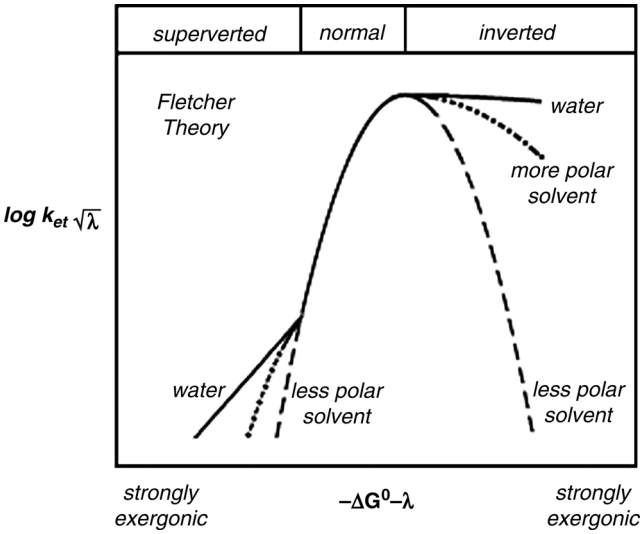


**Figure 1.7** The rate constant for electron transfer ($k_{ET}$) as a function of the driving force ($-\Delta G^0$) and reorganization energy ($\lambda$) on the Fletcher theory [71, 72]. Note the powerful catalytic effect of polar solvents (such as water) on strongly exergonic reactions.

theory, the relative permittivity of the environment exerts a powerful influence on the reaction rate in the highly exergonic region (the "inverted" region) and in the highly endergonic region (the "superverted" region).

According to authors, nonadiabatic electron transfer is expected to be observed whenever there is small orbital overlap (weak coupling) between donor and acceptor states, so that overall electron transfer rates are slow compared to the media dynamics. For strongly exergonic electron transfer reactions that are activated by charge fluctuations in the environment, the activation energy was determined by the intersection point of thermodynamic potentials (Gibbs energies) of the reactants and products. The following equations for $G_{\text{reactants}}$ and $G_{\text{products}}$, which are the total Gibbs energies of the reactants and products (including their ionic atmospheres), respectively, were suggested:

$$G_{\text{reactants}} = \frac{1}{2}Q_1^2\left(\frac{1}{4\pi\varepsilon_0}\right)\left(\frac{1}{\varepsilon(0)}\right)\left(\frac{1}{\alpha_{\text{D}}}+\frac{1}{\alpha_{\text{A}}}-\frac{2}{d}\right) \tag{1.13}$$

$$G_{\text{products}} = \frac{1}{2}Q_2^2\left(\frac{1}{4\pi\varepsilon_0}\right)\left(\frac{1}{\varepsilon(\infty)+f_1\,[\varepsilon(0)-\varepsilon(\infty)]}\right)\left(\frac{1}{\alpha_{\text{D}}}+\frac{1}{\alpha_{\text{A}}}-\frac{2}{d}\right) \tag{1.14}$$

$Q_1$ and $Q_2$ are the charge fluctuations that build up on them, $\varepsilon(0)$ is the relative permittivity of the environment in the low-frequency limit (static dielectric constant), $\varepsilon(\infty)$ is the relative permittivity of the environment in the high-frequency limit ($\varepsilon \approx 2$), $a_{\text{A}}$ is the radius of the acceptor in the transition state (including its ionic atmosphere), $a_{\text{D}}$ is the radius of the electron donor in the transition state (including its ionic

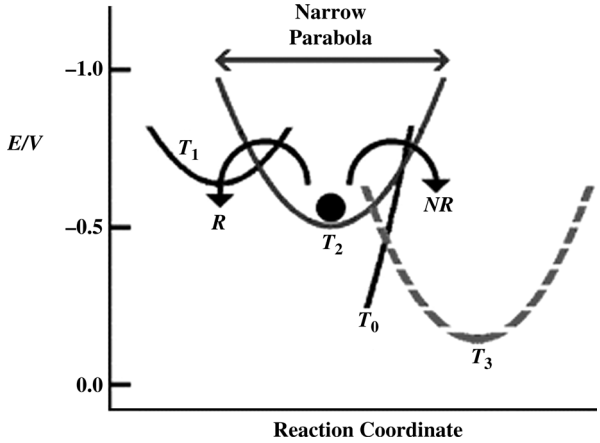


**Figure 1.8** Superimposed Gibbs energy profiles in the vicinity of the electron trap $T_2$. Trapping is thermodynamically reversible, so the electron can return to $T_0$ radiatively (R) via $T_1$ or nonradiatively (NR) via the inverted region. Both routes are kinetically hindered by the extreme narrowness of the Gibbs energy parabola, however. This narrowness is conferred by the extremely nonpolar environment surrounding $T_2$. Trapping state $T_3$ is the final acceptor [72].

atmosphere), and $f_1$ is a constant ($0 < f_1 < 1$) that quantifies the extent of polar screening by the environment, $d$ is the distance between the electron donor and acceptor. Figure 1.8 shows the Gibbs energy for electron transfer through an intermediate.

Authors of paper [73] focused on the microscopic theory of intramolecular electron transfer rate. They examined whether or not and/or under what conditions the widely used Marcus-type equations are applicable to displaced–distorted (D-D) and displaced–distorted–rotated (D-D-R) harmonic oscillator (HO) cases. For this purpose, the cumulant expansion (CE) method was applied to derive the ET rate constants for these cases. In the CE method, the analytical condition was derived upon which the Marcus-type equation of the Gaussian form was obtained for the D-D HO case. In the frame of theory, the following equation for the ET rate constant was derived:

$$W_{b\to a} = \frac{|J_{ab}|^2}{\hbar^2}\sqrt{\frac{\pi\hbar^2}{\lambda k_B T}}\exp\left(-\frac{[\hbar\omega_{ab} + \langle V_{ab}(0)\rangle - \lambda + \lambda]^2}{4\lambda k_B T}\right) \tag{1.15}$$

where $\Delta G_{ab} = \hbar\omega_{ab} + \langle V_{ab}(0)\rangle - \lambda$ and $\hbar\omega_{ab} = E_a - E_b$.

The quantity $\hbar\omega_{ab} + \langle V_{ab}(0)\rangle$ has the following physical meaning. The quantity $\langle V_{ab}(0)\rangle$ is the vibrational energy acquired in the final state through vertical or FC transition from the initial state, averaged over the initial vibrational states under condition of vibrational thermal equilibrium in the initial potential energy surface.

It was found that the reorganization energy and the free energy change for the D-D HO depend on the temperature. As a consequence, the preexponential factor of the ET rate shows a temperature dependence different from the usual Arrhenius

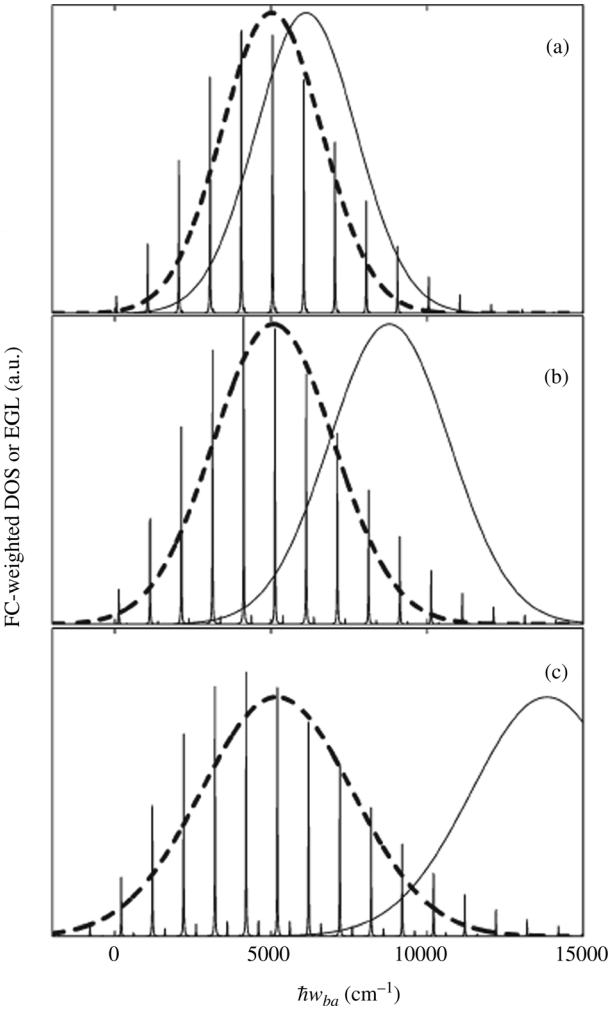


**Figure 1.9** The dependent of the Franck–Condon weighted density 1 (FC DOS) (*y*-axis) on the degree of distortion for a model one-mode D-D HO system described in the text. The degrees of distortion are 0.9 in (a), 0.75 in (b), and 0.6 in (c). The peaks are the EGL calculated with the exact TCF method. The thick dashed lines denote the energy gap law (EGL) of the ET rate EGL calculated with the CE method using the same parameters. The thin smooth lines are the EGL calculated with the conventional Marcus theory [73].

behavior. The dependence of the Franck–Condon weighted density 1 on the degree of distortion for a model one-mode D-D HO system is presented in Figure 1.9.

The temperature dependence of the ET rate at different degrees of mixing for two modes whose frequencies are 100 and 30 $cm^{-1}$ is shown in Figure 1.10.

The influence of spatial charge redistribution modeled by a change in the dipole moment of the reagent that experiences excitation on the dynamics of ultrafast

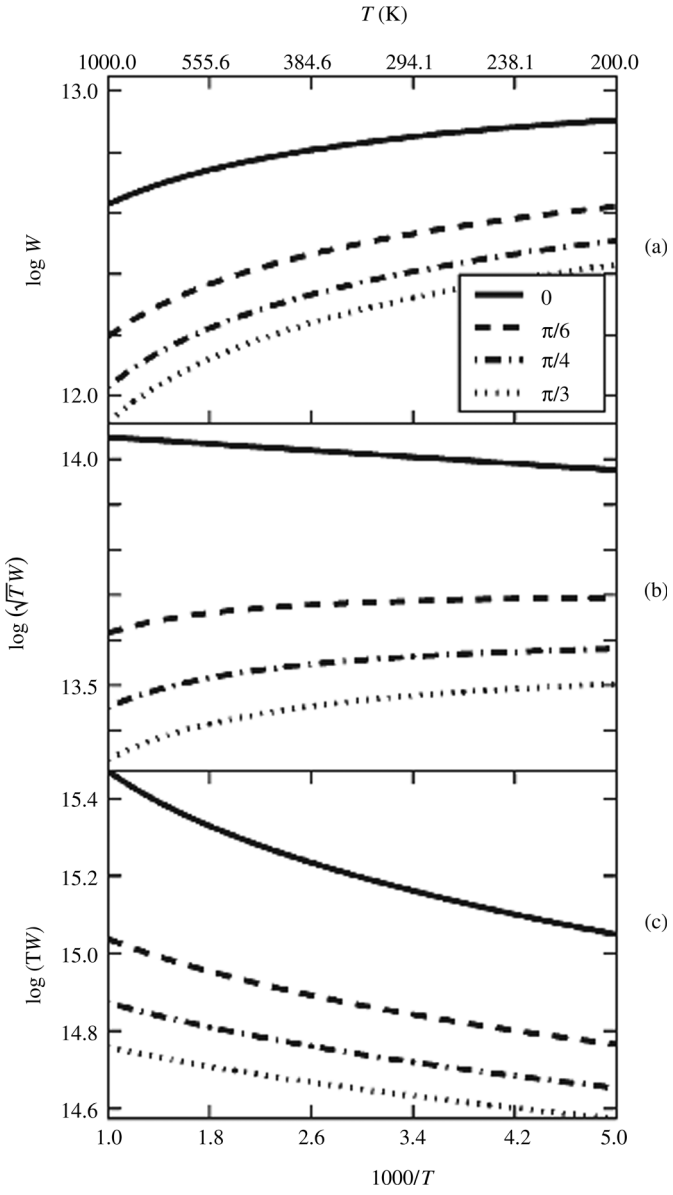


**Figure 1.10** The temperature dependence of the ET rate at different degrees of mixing for two modes whose frequencies are 100 and 30 $cm^{-1}$ in the lower level, without distortion. The abscissa is the inverse temperature, labeled in 1000/T. On the top, *T* (K) is also shown. (a) The ET rate on logarithmic scale versus the inverse temperature, for four different angles of rotation (labeled in the legend in radian). (b) The ET rate multiplied by the square root of the temperature, on logarithmic scale, versus the inverse temperature. (c) The ET rate multiplied by the temperature, on logarithmic scale, versus the inverse temperature [73].

photoinduced electron transfer was studied [22]. A two-center model based on the geometry of real molecules was suggested. The model described photoexcitation and subsequent electron transfer in a donor–acceptor pair. The rate of electron transfer was shown to depend substantially on the dipole moment of the donor at the photoexcitation stage and the direction of subsequent electron transfer. The authors of the work [74] have shown that the polarization fluctuation and the energy gap formulations of the reaction coordinate follow naturally from the Marcus theory of outer electron transfer. The Marcus formula modification or extension led to a quadratic dependence of the free energies of the reactant and product intermediates on the respective reaction coordinates. Both reaction coordinates are linearly related to the Lagrangian multiplier $m$ in the Marcus theory of outer sphere electron transfer, so that $m$ also plays the role of a natural reaction coordinate. When $m = 0$, $F^*(m = 0)$ is the equilibrium free energy of the reactant intermediate $X^*$ at the bottom of its well, and when $m = -1$, $F(m = -1)$ is the corresponding equilibrium free energy of the product intermediate X. $Atm = -1$ the free energy of reorganization of the solvent from its equilibrium configuration at the bottom of the reactant. A theory of electron transfer with torsionally induced non-Condon (NC) effects was developed by Jang and Newton [69]. The starting point of the theory was a generalized spin-boson Hamiltonian, where an additional torsional oscillator bilinearly coupled to other bath modes causes a sinusoidal non-Condon modulation. Closed form time-dependent nonadiabatic rate expressions for both sudden and relaxed initial conditions, which are applicable for general spectral densities and energetic condition, were derived. Under the assumption that the torsional motion is not correlated with the polaronic shift of the bath, simple stationary limit rate expression was obtained. Model calculation of ET illustrated the effects of torsional quantization and gating on the driving force and temperature dependence of the electron transfer rate. The Born–Oppenheimer (BO) formulation of polar solvation is developed and implemented at the semiempirical (PM3) CI level, yielding estimation of ET coupling elements ($V_0$) for intramolecular ET in several families of radical ion systems [70]. The treatment yielded a self-consistent characterization of kinetic parameters in a two-dimensional solvent framework that includes an exchange coordinate. The dependence of $V_0$ on inertial solvent contributions and on donor–acceptor separation was discussed (see Figure 1.11).

In the work [76], it was demonstrated that constrained density functional theory allowed to compute the three key parameters entering the rate constant expression: the driving force ($\Delta G^0$), the reorganization energy ($\lambda$), and the electronic coupling $H_{DA}$. The results confirm the intrinsic exponential behavior of the electronic coupling with the distance separating D and A or, within the pathway paradigm, between two bridging atoms along the pathway. Concerning the "through space" decay factors, the CDFT results suggested that a systematic parameterization of the various kinds of weak interactions encountered in biomolecules should be undertaken in order to refine the global "through space" decay factors. Such a work has been initiated in this paper. The hydrogen bond term has also been adjusted. Besides the refinement of the distance component, the authors underlined the appearance of an angular dependence and the correlation factor between $R$ and $\phi$.

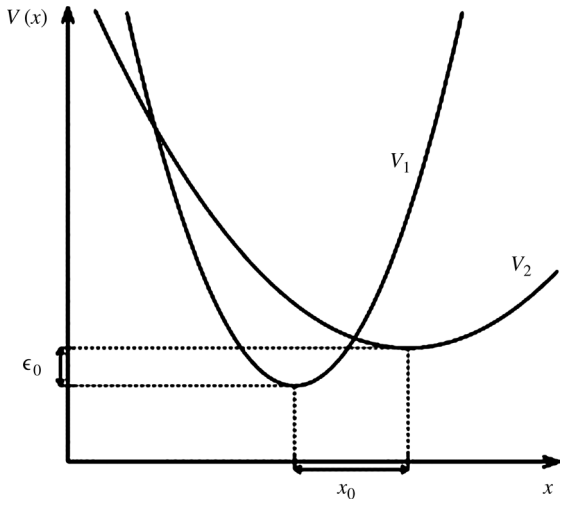


**Figure 1.11** ET dynamics in a low temperature case for different reorganization energies (see details in Ref. [87, 88]).

Taking into account the volume of reagents, the theory gives the following Equation 1.16 [77]:

$$\lambda = \frac{e^2}{2}\left(\frac{1}{n^2} - \frac{1}{e_0}\right)\left(\frac{1}{r_{D^+}} + \frac{1}{r_{A^-}} - \frac{2}{R_{DA}} + \frac{\left[r_{D^+}^3 + r_{A^-}^3\right]}{2R_{DA}^4}\right) \tag{1.16}$$

Further development of theory of reorganization energy consisted in taking into consideration the properties of medium and manner in which it interfaces with the solute [65]. These properties must include both size and shape of the solute and solvent molecules, distribution of electron density in reagents and products, and the frequency domain appropriate to medium reorganization. When the symmetry of donor and acceptor is equivalent, reorganization energy can be generalized as

$$\lambda = C\Delta g_{\text{eff}}(e^2)\left(\frac{1}{r_{\text{eff}}} - \frac{1}{R_{DA}}\right) \tag{1.17}$$

where $C = 0.5$ is a coefficient, $\Delta g_{\text{eff}}$ is the effective charge, and $r_{\text{eff}}$ is the effective radius of charge separated centers. More general theory of the reorganization energy takes the difference between energies of the reactant state and product state, $U_R$ and $U_P$, with the same nuclear coordinates $q$, as the reaction coordinate [78]:

$$\Delta e(q) = U_P(q) - U_R(q) \tag{1.18}$$

In this theory, the reorganization energy is related to the equilibrium mean square fluctuation of the reaction coordinate as

$$L = \frac{1}{2}(\beta < \Delta e - \langle \Delta e \rangle)^2 \tag{1.19}$$

The atoms in the systems are divided into four groups: donor (D) and acceptor (A) sites of a reaction complex (as in protein), nonredox site atoms, and water atoms as the environment. The following calculation determined each component's contribution to $\Delta e$ and, therefore, to the reorganization energy. In the case of thermal excitation of the local molecular and medium high-frequency modes, before theories mentioned predicted the classical Marcus relation in the normal Marcus region. While in the inverted region, significant deviation in the parabolic energy gap dependence is expected. The inverted Marcus region cannot be experimentally observed if the stabilization of the first electron transfer product for the accounting of the high-frequency vibrational mode occurs faster than the equilibrium of the solvent polarization with the momentary charge distribution can be established. Another source of the deviation is the nonparabolic shape of the activation barrier.

The effect of solvent fluctuations on the rate of electron transfer reactions was considered using linear expansion theory and a second-order cumulant expansion [79]. An expression was obtained for the rate constant in terms of the dielectric response function of the solvent and was proved to be valid not only for approximately harmonic systems such as solids but also for strongly molecularly anharmonic systems such as polar solvents.

Microscopic generalizations of the Marcus nonequilibrium free energy surfaces for the reactant and the product, constructed as functions of the charging parameter, were presented [55]. Their relation to surfaces constructed as functions of the energy gap is also established. The Marcus relation was derived in a way that clearly shows that it is a good approximation in the normal region even when the solvent response is significantly nonlinear. The hybrid molecular continuum model for polar solvation, combining the dielectric continuum approximation for treating fast electronic (inertialess) polarization effects, was considered [32]. The slow (inertial) polarization component, including orientational and translational solvent modes, was treated by a combination of the dielectric continuum approximation and a molecular dynamics simulation, respectively. This approach yielded an ensemble of equilibrium solvent configurations adjusted to the electric field created by a charged or strongly polar solute. Both equilibrium and nonequilibrium solvation effects were studied by means of this model, and their inertial and inertialess contributions were separated. Three types of charge transfer reactions were analyzed. It was shown that the standard density linear response approach yields high accuracy for each particular reaction, but proves to be significantly in error when reorganization energies of different reactions were compared.

### 1.2.3
### Zusman Model and its Development

The Zusman equation (ZE) has been widely used to study the effect of solvent dynamics on electron transfer reactions [80–90]. In this equation, dynamics of the electronic degrees of freedom is coupled to a collective nuclear coordinate. Application of this equation is limited by the classical treatment of the nuclear degrees of

freedom. The Zusman theory is based on description of the solvent complex permittivity in the Debey approach. According to the theory, the Gibbs energy activation

$$\Delta G^{\neq} = (\Delta G_0 + E_p)^2/4E_p \tag{1.20}$$

where

$$E_p = (8\pi)^{-1}(1/\varepsilon_m - 1/\varepsilon_s)\ \mathrm{Int}\,\Delta D^2(r)\mathrm{d}r \tag{1.21}$$

where $\varepsilon_m$ is the dielectric constant of the solvent at intermediate frequency, $\varepsilon_s$ is the dielectric constant of the solvent, and $\Delta D(r)$ is the difference of inductions in the first and second dynamics state. The difference of the Equations 1.20 and 1.21 from the corresponding classic Marcus equation (1.5) is that the "equilibrium" reorganization energy $\lambda$ was replaced for the dynamic reorganization energy ($E_p$) of the slow degree of freedom of the solvent, while preexponential factor for nonadiabatic reaction including the coupling factor ($V$) and effective frequency $\upsilon_{ef}$ of the solvent $1/\upsilon_{ef} = \varepsilon_s/\varepsilon_{op}\tau_D$, where $\varepsilon_{op}$ is the optical dielectric constant and $\tau_D$ is the average time for orientation of dipoles of solvent. The Zusman theory is limited because of the neglection of quantum effects in describing the dynamics of the nuclear degrees of freedom.

The authors of paper [84] derived the ZE as a high-temperature approximation to the exact theory. In this work, the authors applied the recently developed hierarchical equations of motion (HEOM) method. A multistate displaced oscillator system strongly coupled to a heat bath was considered a model of an ET reaction system [85]. By performing canonical transformation, the model was reduced to the multistate system coupled to the Brownian heat bath defined by a nonohmic spectral distribution. For this system, the hierarchy equations of motion for a reduced density operator was derived. To demonstrate the formalism, the time-dependent ET reaction rates for a three-state system were calculated for different energy gaps. An analytic study of the density matrix and Wigner representation equations for dissipative electron transfer was presented [86]. Obtained expression showed a very fast relaxation in time if the barrier to reaction is greater than the thermal energy. The fast off-diagonal relaxation disallows an adiabatic elimination of the momentum even in the large friction limit. These equations are a generalization to phase space of the large friction Zusman equations [80]. Taking into account the quantum effect of nuclear dynamics, formalism provided an exact solution to the ET dynamics.

By taking into account both the quantum fluctuations of the collective bath coordinate and its non-Markovian dynamics, an exact solution to the ET dynamics was provided [88]. The forward ET reaction rates were calculated using the HEOM, the ZE, and also the Fermi' golden rule, resulting in

$$k^{FGR} = 2V^2\ \mathrm{Re}\int_0^\infty \mathrm{d}t e^{-iE_0 t}\exp\left[-\int_0^\infty \mathrm{d}\omega\,\frac{4J(\omega)}{\pi\omega^2} \times\{\coth(\beta\omega/2)\,[1-\cos(\omega t)] - i\sin(\omega t)\}\right] \tag{1.22}$$

The interacting spectral density of the harmonic bath was defined as

$$J(\omega) = \frac{\pi}{2}\sum_i \frac{c_i^2}{\omega_i}\delta\left(\omega - \omega_i\right) \tag{1.23}$$

The solvent reorganization energy is determined as

$$\lambda = \frac{4}{\pi}\int_0^\infty \mathrm{d}\omega\, \frac{J(\omega)}{\omega} \tag{1.24}$$

Using solvent-controlled charge transfer dynamics on diabatic surfaces with different curvatures, the framework of Zusman was theoretically analyzed [88]. A generalization of the nonadiabatic Marcus–Levich–Dogonadze rate expression was obtained for the case of different forward and backward reorganization energies and a corresponding generalization of the Zusman rate expression that bridges between nonadiabatic and solvent-controlled adiabatic electron transfer was provided. The derived analytical rate expressions were compared with the precise numerics. The proposed mechanism consisted of spontaneously arising inhomogeneous in space fluctuation in polarization relaxations to equilibrium, not only via solvent dipoles rotation but also via solvent molecule self-diffusion. This process of polarization diffusion leads to the modulation of electronic energy levels that are now fluctuating faster if only the rotational motions of the solvent dipoles are accounted for. It was found that if the rate of tunneling is large enough, the rate constant of the reaction is controlled by the solvent dynamics and the polarization diffusion also contributes. It is also shown that the contribution of the polarization diffusion can become a dominating one in the solvents with large enough diffusion coefficients.

The theory of electron transfer reactions accounting for the influence of the solvent polarization diffusion on the rate of reaction was developed [82]. It was shown that in the limit when reaction is controlled by the solvent dynamics, the effective frequency of the medium fluctuations consists of the sum of two contributions – the contribution of the solvent dipole rotation and the contribution of the solvent polarization diffusion. The model of charge distribution of the products and reagents of the reaction is suggested. Starting from the Zusman equations to the case of parabolic diabatic curves with different curvatures, a generalized master equation for the populations and formal expressions for their long-time limit was derived [89]. In the limit of very small tunnel splitting, a novel rate formula for the nonadiabatic transitions was obtained. For larger values of the tunnel splitting, the consecutive step approximation leading to a rate formula was used that bridges between the nonadiabatic and the solvent-controlled adiabatic regimes.

In Ref. [84], the Zusman equation in the framework of the exact hierarchical equations of motion formalism was revisited. It was shown that a high-temperature approximation of the hierarchical theory is equivalent to the Zusman equation in describing electron transfer dynamics and the exact hierarchical formalism naturally extends the Zusman equation to include quantum nuclear dynamics at low temperatures. Numerical exact results are also presented for the electron transfer reaction dynamics and rate constant calculation. The authors derived the ZE as a

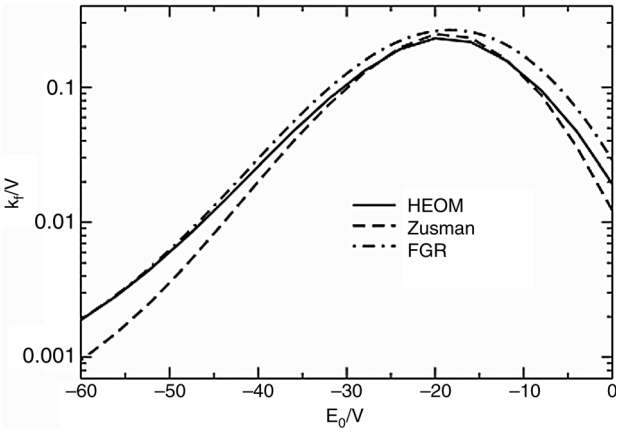


**Figure 1.12** The temperature effect on ET rates derived from different theories (see details in Ref. [84]).

high-temperature approximation to the exact theory, the HEOM method. The latter provides an exact solution to the ET dynamics, by taking into account both the quantum fluctuations of the collective bath coordinate and its non-Markovian dynamics. Since the HEOM method is based on nonperturbative propagation of the reduced density matrix, it can be used to study both nonequilibrium dynamics and dissipative dynamics under a driving laser field interaction. Figure 1.12 shows the temperature effect on ET rates derived from different theories.

It can be seen that the rate from the ZE agrees well with the exact result at high temperatures and deviates from the exact result at low temperatures.

The comprehensive theory of charge transfer in polar media was used for the treatment of experimental data for complex systems, with due account of large-amplitude strongly anharmonic intramolecular reorganization [90]. Equations for the activation barrier and free energy relationships taking into account vibrational frequency changes, local mode anharmonicity, and rotational reorganization, in both diabatic and adiabatic limits were provided. Possible modifications of the Zusman stochastic equations aimed to account for quantum interference of basis states of the system have been investigated. A set of equations that includes nonequilibrium distribution in the momentum space at short timescale in a strong friction limit was obtained. The authors stressed the following features of ET of complex molecules:

1) "Large" intramolecular reorganization, that is, coordinate displacements in excess of, say, $\approx 0.2$ Å;
2) As a consequence of (1), significant vibrational frequency changes (potential surface distortion) and/or large anharmonicity;
3) Intramolecular rotational reorganization;
4) Ion pair reorganization in weakly polar solvents;
5) Multi-ET and long-range ET reactions;
6) All correlations are smooth and appear to resemble one another;

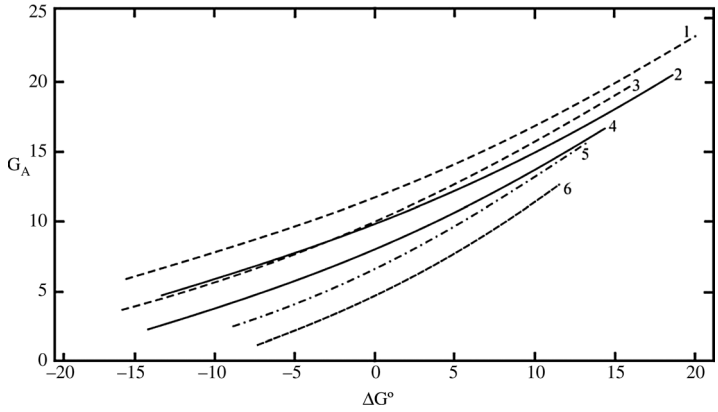


**Figure 1.13** Activation Gibbs free energy dependence on reaction free energy for charge transfer with coupling to a local Morse potential and a harmonic solvent continuum, calculated with different values of the parameter $d$. The harmonic local mode $d = D_f/D_iX_0^2$. Energies in units of $k_BT$, $T = 298$ K. $E_r^{sol} = E_r^{Q} = 20$. Resonance splitting $\Delta E = 4$. The following parametric variations: (1) $d = 2$, diabatic limit; (2) $d = 2$, adiabatic limit; (3) $d = 1$, diabatic limit; (4) $d = 1$, adiabatic limit; (5) $d = 0.5$, diabatic limit; (6) $d = 0.5$, adiabatic limit. Large $d$ corresponds to strong repulsion in the repulsive branch of the Morse potential, small $d$ to weak repulsion. Large $d$ therefore gives the higher activation free energy. $d = D_f/D_iX_0^2$ Morse potential ($d = 0.5$), adiabatic limit [90].

7) The activation free energy increases with increasing $d$, which characterizes the repulsive branches of the Morse potentials in the initial and final states. Small $d$ represents a shallower potential in the final than in the initial state, and vice versa. Smaller values of $d$ therefore give a smaller activation Gibbs free energy (Figure 1.13).

Harmonic and anharmonic potentials were compared. The harmonic local mode corresponds to $d = 1$. The activation free energy for a shallow final-state anharmonic mode ($d = 0.5$) is lower than for the harmonic mode ($d = 1$) but higher for a steep repulsive final state branch ($d = 2$). In addition, the correlation was notably asymmetric around zero driving force for the anharmonic mode, with larger curvature for negative than for positive $\Delta G^0$. Resonance splitting ($\Delta E = 0.1$ and 0.2 eV) lowers the activation free energy by approximately $\Delta E/2$ over most of the driving force range.

$$\alpha = \frac{dG_A}{d\Delta G^0} = \frac{1}{2}\left[1 + \frac{\Delta G^0}{E_i^{sol}}\right] \tag{1.25}$$

### 1.2.4
### Effect of Nonequilibrity on Driving Force and Reorganization

When the initial state distribution remains in thermal equilibrium throughout the ET process, the process driving force is related to the standard Gibbs energy ($\Delta G_0$).

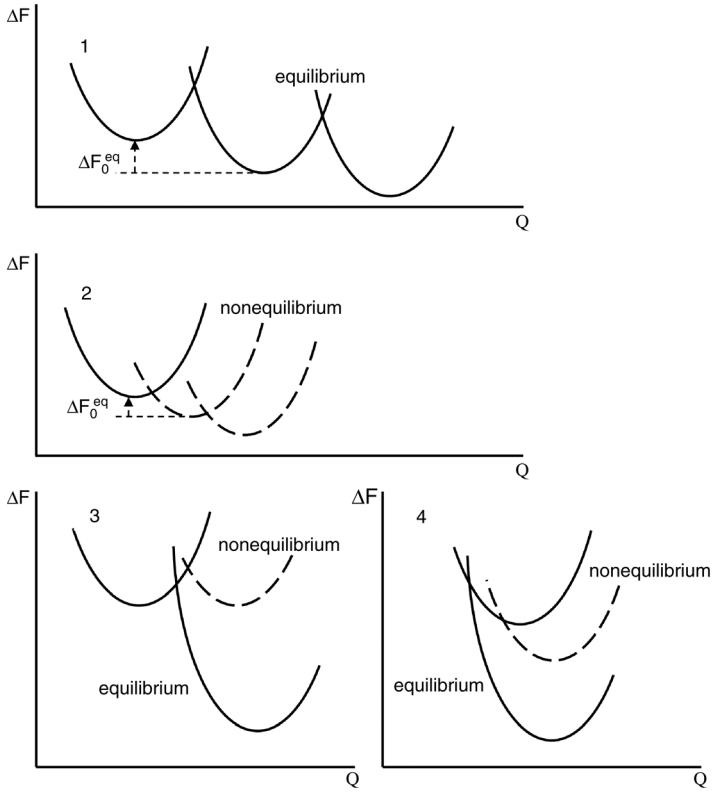


**Figure 1.14** Schematic representation of electronic potential energy surfaces: (1) consecutive conformational and solvational equilibrium processes with the essential change in the nuclear coordinates $Q$ and the standard Gibbs energy $\Delta G_0$; (2) consecutive nonequilibrium processes with small changes in $Q$ and $\Delta G_0$; (3, 4) equilibrium (full line) and nonequilibrium (broken line) processes in the normal and inverted Marcus regions, respectively. Reproduced with permission from Ref. [91].

A different situation takes place if the elementary act of ET occurs before the formation of conformational and solvational states of the medium. In fact, two consecutive stages take place: ET for the accounting of fast vibration translation modes of the system and the media relaxation. In such a case, the thermodynamic standard energy for the elementary act ($\Delta G_0^{neq}$) appears to be less than that involved in the case of the equilibrium dielectric stabilization of redox centers $\Delta G_0$ [9, 19, 91]. It can be concluded that the initial and final energy terms in the nonequilibrium case will be positioned closer to each other in space and energy than in equilibrium (Figure 1.14). Consequently, in the inverted Marcus region, the value of the reorganization, Gibbs and activation energies are expected to be markedly lower than that in the equilibrium case. In the normal Marcus region, we predict a larger activation energy and slower ET rate for nonequilibrium processes than for

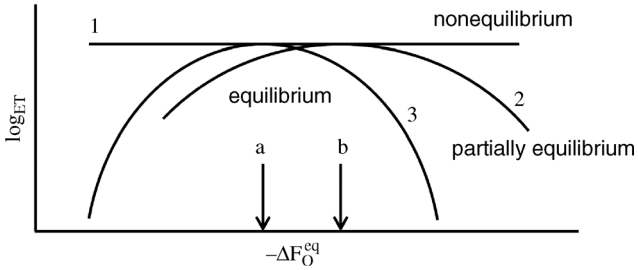


**Figure 1.15** Schematic representation of the dependence of the ET constants logarithm on the equilibrium Gibbs energy $\Delta G_0$: (1) nonequilibrium conformational and solvational processes; (2) partial nonequilibrium processes, $\lambda^{neq}$ and $\Delta G_0^{neq}$, are slightly dependent on $\Delta G_0$; (3) equilibrium processes. Arrows a and b are conditions for the maximum $\lambda = \Delta G_0$ and $\lambda^{neq} = \Delta G_0^{neq}$, respectively. Reproduced with permission from Ref. [91]

equilibrium processes when differences in their standard Gibbs energy would be larger than that in the reorganization energy. In general, the situation would be dependent on the interplay of both parameters of the Marcus model. The second property expected for nonequilibrium processes is the lack of dependence (Figure 1.15, curve 1) or weak dependence (curve 2) of the experimental rate constant of ET in both Marcus regions (inverted and noninverted), compared to that predicted by the classic Marcus expression (curve 3).

During the ET processes, the nuclear degrees of freedom need to reorganize in responding to the change in charge distributions upon the electronic state transitions. The interplay of electronic coupling and nuclear reorganization dynamics could thus result in rich dynamical behaviors in ET reactions. An example of nuclear dynamical effects on ET reaction is that, when increasing the nuclear relaxation time, ET reactions change from the nonadiabatic regime to the solvent-controlled adiabatic regime.

A microscopic theory for the rate of nonadiabatic electron transfer, including generalizations of the Marcus nonequilibrium free energy surfaces for the reactant and the product, was developed and its relation to classical Marcus theory was analyzed [92]. A simple algorithm was proposed for calculating free energy changes from computer simulations on just three states: the reactant, the product, and an "anti"-product formed by transferring a positive unit charge from the donor to the acceptor. The activation energy as a parabolic function of the free energy change of reaction was derived when the solvent response is significantly nonlinear. The electron transfer theory for the high-frequency intramolecular mode and low-frequency medium mode for a single-mode case when the reactant surface is not in a thermal equilibrium has been rederived [93]. In the limit of very low and very high temperatures, the expressions were analyzed and compared with the case of thermal distribution and a Franck–Condon factor for a multimode displaced, distorted, and Duschinsky rotated adiabatic potential surfaces has been derived to obtain the ET rate.

### 1.2.5
### Long-Range Electron Transfer

Long-range Electron Transfer (LRET) between donor (D) and acceptor (A) centers can occur by three mechanisms: (1) direct transfer that involves direct overlap between electron orbitals of the donor and acceptor, (2) consecutive electron jumps via chemical intermediates with a fixed structure, and (3) superexchange via intermediate orbitals. In direct LRET the direct electronic coupling between D and A is negligible and this mechanism is not practically realized in condensed media being noncompetitive with the consecutive and superexchange processes. In theoretical consideration of the consecutive LRET, a relevant theory of ET in two-term systems can be applied.

Of considerable interest is the superexchange process [9, 91, 94–110]. According to the Fermi's golden rule (Equation 1.5), the nonadiabatic ET rate constant is strongly dependent on electronic coupling between the donor state D and the acceptor state A connected by a bridge ($V_{AB}$) that is given by an expression derived from the weak perturbation theory

$$V_{AB} = \frac{\sum V_{A\alpha} V_{\alpha B}}{\Delta E_\alpha} \tag{1.26}$$

where $V_{A\alpha}$ and $V_{\alpha B}$ are the couplings between bridge orbitals and acceptor and donor orbitals, respectively, and $\Delta E_\alpha$ is the energy of the bridge orbitals relative to the energy of the donor orbital. The summation over $\alpha$ includes both occupied and unoccupied orbitals of the bridge.

Using static perturbation theory, time-dependent perturbation theory, and direct time-dependent dynamics within generalized tight binding models, the authors of work [99] examined the role of energy gaps, relative energetics of donor and acceptor orbitals with hole-type and electron-type superexchange sites, damping and dephasing, and overall energetics in electron transfer. The dynamic studies indicated some important phenomena, which include quantum interferences between different pathways, recurrences, and oscillations and competitive effects of hole-type and electron-type superexchange. An integral equation approach to nonlinear effects in the free energy profile of electron transfer reaction has been developed [103]. Electronic and dynamical aspects of superexchange-assisted through-bridge electron transfer were considered. This approach was extended to a more general case, where D is connected to A by a number of atomic orbitals. A special, the so-called "artificial intelligence," search procedure was devised to select the most important amino acid residues, which mediate long-range transfer [104–106].

According to the approach of Onuchic and coworkers [107], for a pathway between bridged donor and acceptor groups, the coupling element can be written as

$$V_{AB} = V_0 \prod_i^N \varepsilon_i \tag{1.27}$$

where $V_0$ is the coupling between the donor and the first bond of the pathway and $\varepsilon_i$ is a decay factor associated with the decay of electron density from one bond to another.

The $\varepsilon_B$, $\varepsilon_H$, and $\varepsilon_s$ values are related to superexchange through two covalent bonds sharing a common atom, an H bond, and space, respectively. The decay factor is approximated by equation

$$\varepsilon_i = \varepsilon_i^0 \exp\left[\beta_i(R - R_i^0)\right] \tag{1.28}$$

where $R_i^0$ is the equilibrium length bond or van der Waals distance, $\beta_i$ is some factor, specific to the distance $R$, which depends on the orbital interactions and $\varepsilon_i^0$ is the value of $\varepsilon_i$ for $R = R_i^0$, which is proportional to factor $\sigma$ related to the interaction orientation. The values of $\varepsilon_B = 0.4$–$0.6$, $\sigma_H = \sigma_B = 1.0$, and $\beta_s = 1.7$ Å were taken for the calculation of $V_{AB}$. According to this theory, the increase in connectivity for the electron transfer is about 0.24 per atom.

A semiempirical approach for the quantitative estimation of the effect bridging the group on LRET was developed by Likhtenshtein [9, 91].

The basic idea underlying this approach is an analogy between superexchange in electron transfer and such electron exchange processes as triplet–triplet energy transfer (TTET) and spin exchange (SE). The ET rate constant is proportional to the square of the resonance integral $V_{ET}$. The rate constant of TTET is

$$k_{TT} = \frac{2\pi}{h} J_{TT} \mathrm{FC} \tag{1.29}$$

where $J_{TT}$ is the TT exchange integral. The Hamiltonian of the exchange interaction ($H_{SE}$) between spins with operators $S_1$ and $S_2$ is described by the equation

$$H_{SE} = -2J_{SE} S_1 S_2 \tag{1.30}$$

where $J_{SE}$ is the SE exchange integral.

All three integrals $V_{ET}^2$, $J_{SE}$, and $J_{TT}$ are related to the overlap integral ($S_i$), which quantitatively characterizes the degree of overlap of orbitals involved in these processes. Thus,

$$V_{ET}^2, J_{SE}, J_{TT} \propto S_i^n \propto \exp(-\beta_i R_i) \tag{1.31}$$

where $R_i$ is the distance between the interacting centers and $\beta_i$ is a coefficient that characterizes the degree of the integral decay. In the first approximation, $n = 2$ for the ET and SE processes with the overlap of two orbitals and $n = 4$ for the TT process in which four orbitals overlap (ground and triplet states of the donor and ground and triplet states of the acceptor). The spin exchange and TT phenomena may be considered an idealized model of ET without or with only a slight replacement of the nuclear frame (see Figure 1.16). Thus, the experimental dependence of exchange parameters $k_{TT}$ and $J_{SE}$ on the distance between the exchangeable centers and the chemical nature of the bridge connecting the centers may be used for evaluating such dependences for the resonance integral in the ET equation (1.30).

A vast literature is connected with the quantitative investigation of exchange processes [101, 102]. As it seen in Figure 1.17, experimental data on the dependence of $k_{TT}$ and $J_{SE}$ on the distance between the centers ($\Delta R$) lie on two curves, which are approximated by the following equation [91].

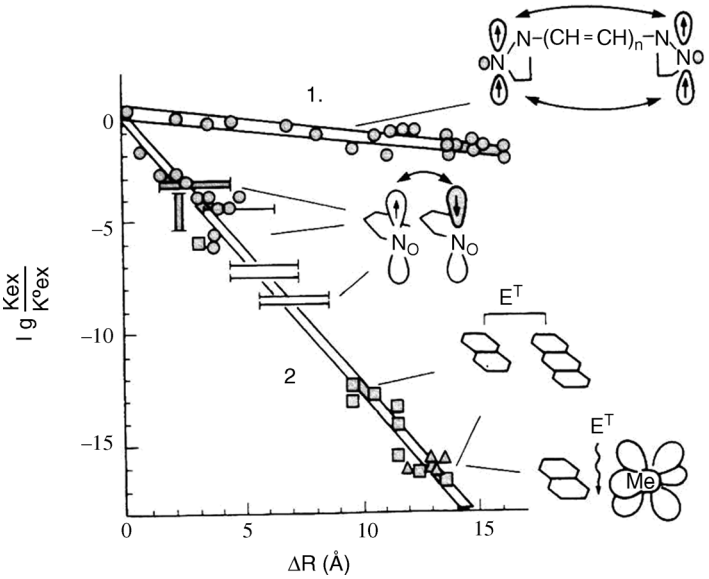


**Figure 1.16** Dependence of the logarithm of relative parameters of the exchange interaction on the distance between the interacting centers ($\Delta R$). $k_{TT}$ is the rate constant of triplet–triplet electron transfer and JSE is the spin-exchange integral. Index 0 is related to van der Waals contact. Reproduced with permission from Ref. [91].

$$k_{TT}, J_{SE} \propto \exp(-\beta \Delta R) \tag{1.32}$$

For systems in which the centers are separated by a "nonconductive" medium (molecules or groups with saturated chemical bond), $\beta_{TT}$ equals $2.6\,\text{Å}^{-1}$. For systems in which the radical centers are linked by "conducting" conjugated bonds, $\beta_{SE}$ is $0.3\,\text{Å}^{-1}$.

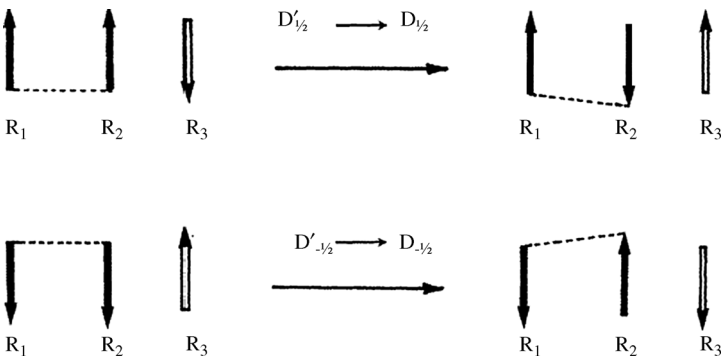


**Figure 1.17** Triplet–singlet spin conversion of the radical pair [110, 112].

We can consider the ratios

$$\gamma_{SE} = \frac{J^0_{SE}}{J_{SE}}(\Delta R) \tag{1.33}$$

as parameters of attenuation of the exchange interaction of SE through the given medium. Taking into account Equations 1.31 and 1.32 with value $n = 2$ for SE and ET, we have an expression for the dependence of the attenuation parameters for SE and ET on the distance between remote donor and acceptor centers $D_R D_A$

$$\gamma_{ET} = \gamma_{SE} = \exp(-\beta_i \Delta R) \tag{1.34}$$

with $\beta_{ET}(nc) = 0.5\beta_{TT} = 1.3\ \text{Å}^{-1}$ for a "nonconducting" medium and $\beta_{ET}(c) = 0.3\ \text{Å}^{-1}$ for a "conducting" bridge. The value of $\beta_{ET}$ ($1.3\ \text{Å}^{-1}$) is found to be close to that obtained by analysis of $k_{ET}$ on the distance $\Delta R$ in model and biological systems (Figure 2.7).

An examination of the empirical data on the exchange integral values ($J_{ET}$) for the spin–spin interactions in systems with known structure, that is, biradicals, transition metal complexes with paramagnetic ligands, and monocrystals of nitroxide radicals, allows the value of the attenuation parameter $\gamma_X$ for the exchange interaction through a given group X to be estimated. By our definition, the $\gamma_X$ is

$$\gamma_X = \frac{J_{RYZP}}{J_{RYXZP}} \tag{1.35}$$

where R is a nitroxide or organic radical, P is a paramagnetic complex or radical, and X, Y, and Z are chemical groups in the bridge between R and P.

Table 1.1 shows the results of the calculation parameter $\gamma_X$ from empirical data by Equation 1.35 [9, 19]. The table of values for X, C=O, S=O, P=O and C=C, calculated from independent experimental data, is similar. Data presented in Table 1.1 and

**Table 1.1** Values of the attenuation parameter of individual groups ($\gamma_X$), van der Waals contact ($\gamma_v$), and hydrogen bond ($\gamma_{hb}$) for spin exchange in biradicals and paramagnetic complexes of transition metals with nitroxide ligands (see text) (reproduced with permission from Ref. [91]).

| Group, X | $\gamma_x$ | Group, X | $\gamma_x$ |
|---|---|---|---|
| $C_6H_4$ | $6.00 \pm 0.03$ | | |
| C=C | 1.7 | −NH−CO− | 55[a] |
| C=O | $8.4 \pm 0.4$ | $\gamma_v$ | 50 |
| C | | | |
| NH | 6.5 | $\gamma_{hb}$ | 10 |
| O | 5 | H | 12 |
| S=O | 2.1 | $SO_2$ | 2.2 |
| | 3.5 | RP=O | $2.40 \pm 0.03$[b] |

a) Calculated by equation $\gamma x = \gamma_{CO}\gamma_{NH}$.
b) R ≡ Ph−, $CH_2$=CH−, Ph−CH=CH−, Ph−CCl=CH−.

Equation 1.35 may be used for the analysis of alternative electron transfer pathways in biological systems.

The dynamics of charge transfer from a photoexcited donor to an acceptor coupled through a bridge was investigated by using a correlation function approach in Liouville space that takes into account solvent dynamics with an arbitrary distribution of timescales [108]. A nonadiabatic theory of electron transfer, which improves the standard theory near the inversion point and becomes equivalent to it far from the inversion point, was presented [109]. This theory revealed the existence of an especially interesting marginal case when the linear and nonlinear coefficients of a two electronic states system are appropriately tuned for forming a coherent electron–phonon oscillator. An electron injected in one of the electronic states of a CEPO generates large amplitude charge oscillations associated with coherent phonon oscillations and electronic-level oscillations that may resonate with a third site that captures the electron so ultrafast electron transfer becomes possible (Figure 1.5). Numerical results are shown where two weakly interacting sites, a donor and a catalyst, form a CEPO that catalytically triggers an UFET to an acceptor.

### 1.2.6
### Spin Effects on Charge Separation

Chemical reactions are known to be controlled by two fundamental parameters, energy (both free and activation energy) and angular momentum (spin) of reactants [110, 111]. The latter results in electron and nuclear spin selectivity of reactions: only those spin states of reactants are chemically active whose total spin is identical to that of products. For example, for the triplet radical pair ($R_1$, $R_2$) prepared by photolysis, radiolysis, or encounter of freely diffusing radicals to recombine and produce diamagnetic, zero-spin molecule $R_1R_2$, triplet–singlet spin conversion of the radical pair is required (Figure 1.17).

In a static model of spin catalysis, if the starting spin state of the pair is triplet (it corresponds to D′ state of the triad), then the probability to find this pair in the singlet state (it corresponds to D state of the triad) [110, 111]:

$$\varrho_S(t) = (\Delta J/2\Omega)\sin^2 \Omega t \tag{1.36}$$

where

$$\Omega = 2^{-1/2}[(J_{12}-J_{13})^2 + (J_{12}-J_{23})^2 + (J_{13}-J_{23})^2]^{1/2} \tag{1.37}$$

and $\Delta J = J_{13} - J_{23}$; $J_{ij}$ denotes the pair-wise exchange energies for pairs $R_i$ and $R_j$ ($i \neq j$), ($i, j = 1, 2, 3$). Both conjugated processes, triplet–singlet conversion of the pair and doublet–doublet evolution of the triad, oscillate in time with a period $\tau = (2\Omega)^{-1}$.

Photogenerated radical pairs are capable of exhibiting coherent spin motion over microsecond timescales, which is considerably longer than coherent phenomena involving photogenerated excited states. The rate of radical pair intersystem crossing between photogenerated singlet and triplet radical pairs has been shown to increase in the presence of stable free radicals and triplet state molecules. Spin catalysis was

proved to operate in radical recombination biradical decay, *cis–trans* isomerization of molecules, primary light-harvesting reactions in photosynthetic centers, charge separation and water oxidation by photosystem II, in particular, paramagnetic quenching of excited molecules, and so on [110]. Another way of controlling the lifetime of the photoseparated charges by the spin chemistry mechanism appears to be the introduction to donor or acceptor molecules an isotope bearing a nuclear spin [111].

### 1.2.7
### Electron–Proton Transfer Coupling

Proton-coupled electron transfer (PCET) reactions play a vital role in a wide range of chemical and biological processes such as the conversion of energy in photosynthesis and respiration, in electrochemical processes, and in solid state materials. Recently, a number of experiments on model PCET systems have been performed [112–123]. A theory of PCET was developed by Cukier and coworkers [113–115]. The authors took in consideration that in PCET the electron and proton may transfer consecutively, electron transfer followed by proton transfer (PT), designated as ET/PT, or they may transfer concertedly, in one tunnel event, designated as ETPT. It was suggested that the proton charge is coupled to the solvent dipoles in a fashion similar to the electron–solvent coupling and the analysis of effect of solvation on the shape of the proton potential energy surface allowed to evaluate the PCET rate constant. The dielectric continuum theory was used to obtain the proton-solvated surfaces. According to this model, the proton can affect the PCET rate via Franck–Condon factors between the proton surfaces for the initial and final electron states and also influence the activation energy via the proton energy levels. The rates corresponding to the ETPT and ET/PT channels were evaluated for several model reaction complexes that mimic electron donor–hydrogen-bonded interface–electron acceptor system parameters. Figure 1.18 displays the charge site geometry and the ellipsoid and spheres with the definitions of the relevant dimensions.

According to the theory, the rate constant is

$$k_{\mathrm{ETPT}} = \frac{V_{\mathrm{el}}^2}{\hbar^2}\sqrt{\pi\hbar^2/\lambda_{\mathrm{s}}^{\mathrm{ETPT}} k_{\mathrm{B}} T} \times \sum_{n'} \varrho_{in'} \sum_{n\in b} |\langle \chi_{fn}|\chi_{in'}\rangle|^2 \times \mathrm{e}^{-(\lambda_{\mathrm{s}}^{\mathrm{ETPT}} + \Delta^{el} + \varepsilon_{fn} - \varepsilon_{in'})^2/4\lambda_{\mathrm{s}}^{\mathrm{ETPT}} k_{\mathrm{B}} T} \tag{1.38}$$

where $\chi_{\mathrm{i}}$ is the protonic wave function, which is dependent on the electron state; $\lambda_{\mathrm{s}}$ is the reorganization energy arising from the solvent–charge coupling and the reaction free energy. The reaction free energy is the sum of the electronic structure $\Delta E^{\mathrm{el}}$ and the equilibrium solvation $\Delta G^{\mathrm{sol}}$ contributions, $\varepsilon_{\mathrm{i}}'$ and $\varepsilon_{\mathrm{f}}'$ are the proton energy in initial and final states, respectively.

In the theory for PCET developed by Hammes-Schiffer and coworkers [116–123], a PCET reaction involving the transfer of one electron and one proton (depicted in Figure 1.19) was described in terms of four diabatic states: the proton and electron on

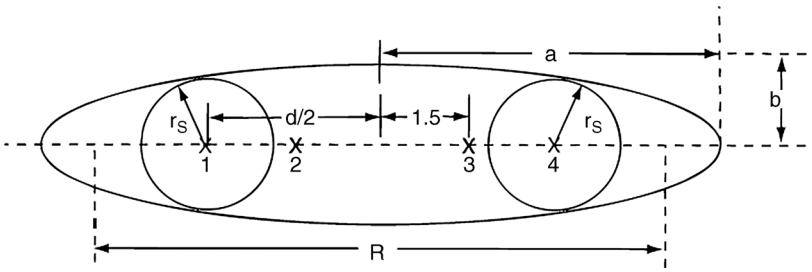


**Figure 1.18** Model for the evaluation of the reorganization and solvation free energy of the ET, PT, and ETPT reactions. The donor and acceptor sites are spheres of radius $r_s$ embedded in an ellipsoid with major (minor) axis *a* (*b*) and interfocal distance *R*. The locations 1 and 4 (2 and 3) denote charge sites associated with the electron (proton) states. The proton sites are at a fixed distance of 3 Å and the electron sites are separated by a distance *d* of 15 Å. The ellipsoid expands to contain the donor and acceptor spheres as the sphere radii increase [113].

their donors, the proton and electron on their acceptors, the proton on its donor and the electron on its acceptor, and the proton on its acceptor and the electron on its donor. The transferring hydrogen nucleus was treated quantum mechanically to include effects such as zero point energy and hydrogen tunneling.

Within this four-state model, the mixed electron/proton vibrational free energy surfaces were obtained as functions of two collective solvent coordinates corresponding to ET and PT and the free energy surfaces for PCET reactions were approximated as two-dimensional paraboloids (Figure 1.20).

In this case, the PCET reaction is viewed as a transition from the reactant set of paraboloids to the product set of paraboloids. Thus, this theory is a multidimensional analogue of standard Marcus theory for single ET and the PCET reaction requires a reorganization of the solvent and involving intramolecular solute modes.

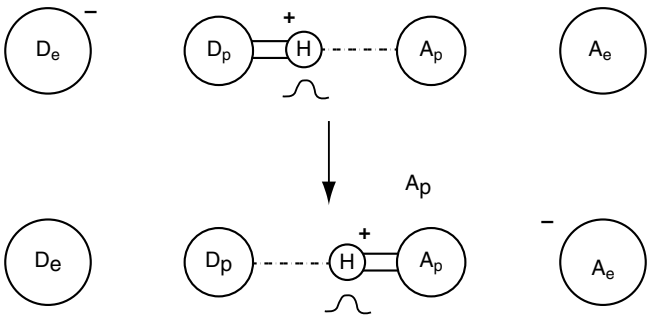


**Figure 1.19** Schematic illustration of a PCET reaction, where the electron donor and acceptor are denoted $D_e$ and $A_e$, respectively, and the proton donor and acceptor are denoted $D_p$ and $A_p$, respectively. The transferring proton is represented as both a sphere and a quantum mechanical wave function [120].

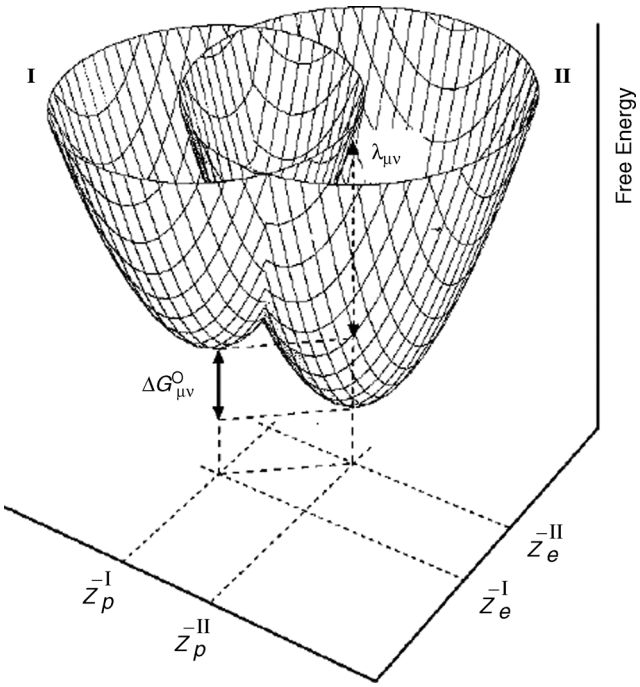


**Figure 1.20** Schematic illustration of a pair of paraboloids Iμ and IIν as functions of the solvent coordinates $z_p$ and $z_e$. The reorganization energy $\lambda_{\mu\nu}$ and the equilibrium free energy difference $\Delta G^{0}_{\mu\nu}$ are indicated [120].

The theoretical description of the most basic PCET reaction involved the transfer of one electron and one proton requires four diabatic states:

$$(1a)\quad D_e^{\ominus} - {}^{\oplus}D_pH \cdots A_p - A_e$$

$$(1b)\quad D_e^{\ominus} - D_p \cdots HA_p^{\oplus} - A_e$$

$$(2a)\quad D_e - {}^{\oplus}D_pH \cdots A_p - A_e^{\dot{A}}$$

$$(2b)\quad D_e - D_p \cdots HA_p^{\oplus} - A_e^{\dot{A}}$$

According to Ludlow *et al.* [122], there are three distinct regimes of PCET:

1) Electronically adiabatic PT and ET, where the coupling between all pairs of the four diabatic states is strong.
2) Electronically nonadiabatic PT and ET, where the coupling between all pairs of the four diabatic states is weak.
3) Electronically adiabatic PT and electronically nonadiabatic ET, where the coupling between PT diabatic states is strong and the coupling between ET diabatic states is weak.

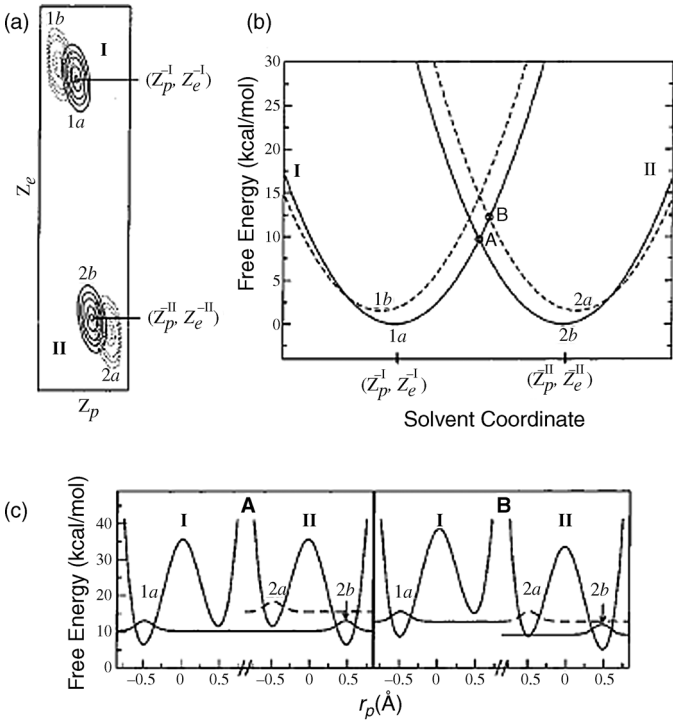


**Figure 1.21** (a) Schematic illustration of two-dimensional ET diabatic mixed electronic/proton vibrational free energy surfaces as functions of the solvent coordinates $z_p$ and $z_e$. The reactant and product ET diabatic surfaces are labeled I and II, respectively. Only two surfaces are shown for each ET diabatic state, and the lower and higher energy surfaces are shown with solid and dashed contour lines, respectively. Each free energy surface is labeled according to the dominant diabatic state, and the minima of the lowest surfaces are labeled $(\bar{z}_p^{I}, \bar{z}_e^{I})$ and $(\bar{z}_p^{II}, \bar{z}_e^{II})$. (b) Slices of the free energy surfaces along the straight-line reaction path connecting solvent coordinates $(\bar{z}_p^{I}, \bar{z}_e^{I})$ and $(\bar{z}_p^{II}, \bar{z}_e^{II})$ indicated in (a). Only the lowest surface is shown for the reactant (I), and the lowest two surfaces are shown for the product (II). (c) The reactant (I) and product (II) proton potential energy curves are functions of $r_p$ at the solvent configurations corresponding to the intersection points A and B indicated in (b) [120].

The regime of electronically adiabatic PT and electronically nonadiabatic ET is suggested to be most relevant for PCET reactions with a well-separated electron donor and acceptor connected by a hydrogen-bonded interface. Schematic illustration of two-dimensional ET diabatic mixed electronic/proton vibrational free energy surfaces as functions of the solvent coordinates $z_p$ and $z_e$ is displayed in Figure 1.21.

A rate expression in the limit of electronically adiabatic PT and electronically nonadiabatic was derived. Application of the golden rule to the two sets of free energy surfaces illustrated in Figure 1.5a leads to the following rate expression:

$$k = \frac{2\pi}{\hbar} \sum_{\mu} P_{l\mu} \sum_{\nu} V_{\mu\nu}^2 \left(4\pi\lambda_{\mu\nu} k_B T\right)^{-1/2} \exp\left\{\frac{-(\Delta G_{\mu\nu}^0 + \lambda_{\mu\nu})^2}{4\lambda_{\mu\nu} k_B T}\right\} \tag{1.39}$$

where $\sum_{\mu}$ and $\sum_{\nu}$ indicate a sum over vibrational states associated with ET states 1 and 2, respectively, and $P_{I\mu}$ is the Boltzmann factor for state $I_{\mu}$. In this expression, the reorganization energy is defined as

$$\lambda_{\mu\nu} = \varepsilon_{\mu}^{I}\left(\bar{z}_{p}^{II_{\nu}}, \bar{z}_{e}^{II_{\nu}}\right) - \varepsilon_{\mu}^{I}\left(\bar{z}_{p}^{I_{\mu}}, \bar{z}_{e}^{I_{\mu}}\right) = \varepsilon_{\nu}^{II}\left(\bar{z}_{p}^{I_{\mu}}, \bar{z}_{e}^{I_{\mu}}\right) - \varepsilon_{\nu}^{II}\left(\bar{z}_{p}^{II_{\nu}}, \bar{z}_{e}^{II_{\nu}}\right) \tag{1.40}$$

and the free energy difference is defined as

$$\Delta G_{\mu\nu}^{0} = \varepsilon_{\nu}^{II}(\bar{z}_{p}^{II\nu}, \bar{z}_{e}^{II\nu}) - \varepsilon_{\mu}^{I}(\bar{z}_{p}^{I\mu}, \bar{z}_{e}^{I\mu}) \tag{1.41}$$

where $(\bar{z}_{p}^{I_{\mu}}, \bar{z}_{e}^{I_{\mu}})$ and $(\bar{z}_{p}^{II_{\nu}}, \bar{z}_{e}^{II_{\nu}})$ are the solvent coordinates for the minima of $\varepsilon_{\mu}^{I}(z_p, z_e)$ and $\varepsilon_{\nu}^{II}(z_p, z_e)$, respectively. As a result of the averaging over, the proton applicability of the Born–Oppenheimer approximation (BOA) for the calculation of the transition probability for a nonadiabatic process of charge transfer in a polar environment with allowance made for temperature effects was theoretically investigated.

The transfer of a quantum particle (proton) that interacts with a local vibration mode in a model of bound harmonic oscillators was considered [124]. The model admitted an exact solution for wave functions of the initial and final states. A calculation showed that the model is applicable even for very large distances of the proton transfer. It was shown that the non-Condon effects are in general temperature dependent and may substantially influence the calculated values of the transition probability.

### 1.2.8
### Specificity of Electrochemical Electron Transfer

The current flowing in either the reductive or oxidative steps of a single electron transfer reaction between two species (O) and (R)

$$O(s) + e^{-}(m) \underset{k_{ox}}{\overset{k_{red}}{\rightleftharpoons}} R(s) \tag{1.42}$$

can be described using the following expressions:

$$i_a = -FAk_{ox}[R]_0 \tag{1.43}$$

$$i_c = -FAk_{red}[O]_0 \tag{1.44}$$

where $i_c$ and $i_a$ are the reduction and oxidation reaction currents, respectively; $A$ is the electrode area; $k_{Red}$ or $k_{Ox}$ are the rate constant for the electron transfer; and $F$ is the Faraday's constant.

At consideration processes occurring with participation of electrodes, the conception of the Fermi energy, Fermi level, and the Fermi–Dirac (F–D) distribution are widely used (http://en.wikipedia.org/wiki/Fermi_energy) [125–128]. The Fermi energy is the energy of the highest occupied quantum state in a system of fermions at absolute zero temperature (http://en.wikipedia.org/wiki/Fermi_energy). By definition, fermions are particles that obey Fermi–Dirac statistics: when one swaps two

fermions, the wave function of the system changes sign. Fermions can be either elementary, like the electron, or composite, like the proton. F–D statistics describes the energies of single particles in a system comprising many identical particles that obey the Pauli exclusion principle. For a system of identical fermions, the average number of fermions in a single-particle state i, is given by the F–D distribution,

$$\bar{n}_{\mathrm{i}} \frac{1}{\mathrm{e}^{(\varepsilon_{\mathrm{i}}-\mu)/kT}+1} \tag{1.45}$$

where $k$ is Boltzmann constant, $T$ is the absolute temperature, $\varepsilon_{\mathrm{i}}$ is the energy of the single-particle state i, and $\mu$ is the chemical potential. At $T=0$, the chemical potential is equal to the Fermi energy. For the case of electrons in a semiconductor, $\mu$ is also called the Fermi level.

The one-dimensional infinite square well of length $L$ is a model for a one-dimensional box. In the framework of a standard model-system in quantum mechanics for a single quantum number $n$, the energies are given by

$$E_n = \frac{\hbar^2\pi^2}{2mL^2}n^2 \tag{1.46}$$

(http://hyperphysics.phy-astr.gsu.edu/HBASE/quantum/disfd.html#c2)

A number of theoretical research studies were devoted to electron transfer reaction from a superconducting electrode [129–142]. The theory of electron transfer reaction from a superconducting electrode that was described in the framework of the resonance valence bond model to a reagent in solution was developed [130]. It was shown that current–overpotential dependence at the boundary between an electrode and solution should be asymmetrical and the current between a superconducting electrode and solution should be substantially suppressed in comparison with that calculated for the same electrode in the normal state.

The quantum theory of electron transfer reactions at metal electrodes was developed [131]. The obtained potential dependence of the electron transfer rate in the weak coupling case was shown to resemble the Butler–Volmer equation of classical electrochemistry. The volcano-shaped dependence of the hydrogen exchange current on the adsorption energy of hydrogen on various metals and the mechanism of hydrogen evolution were explained microscopically. The exchange current density for hydrogen evolution at Pt electrode calculated quantitatively agreed well with the experimental value. Free energy profiles governing electron transfer from a reactant to an electrode surface in water were investigated, based on the reference interaction site model (Figure 1.22) [132]. Three models of a redox pair for charge separation reactions were examined: a pair of atomic solutes and systems consisting of an atom and a surface with a localized or a delocalized electron. It was found that the profile becomes highly asymmetrical when an electron in the electrode is delocalized.

Theoretical analysis of asymmetric Tafel plots and transfer coefficients for electrochemical proton-coupled electron transfer (EPCET) was performed [122]. The input quantities to the heterogeneous rate constant expressions for EPCET were

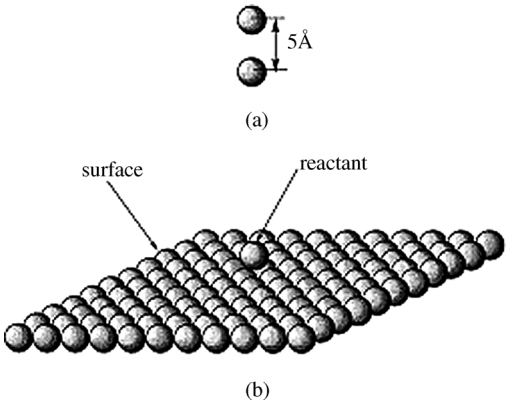


**Figure 1.22** Models of CS electron transfer. (a) A one-site electron donor and a one-site electron acceptor. (b) A two-dimensional array consisting of 121 identical atoms whose structure is land a one-site electron donor that is 5 Anstrem apart from the central atom of the surface [132].

calculated with density functional theory in conjunction with dielectric continuum models. The theoretical calculation indicated that the asymmetry of the Tafel plot (the dependence of electric current on electrode potential) and the deviation of the transfer coefficient at zero overpotential from the standard value of one-half arise from the change in the equivalent proton donor–acceptor distance upon electron transfer. The magnitude of these effects was obtained by the magnitude of this distance change, as well as the reorganization energy and the distance dependence of the overlap between the initial and the final proton vibrational wave functions. This theory provided experimentally testable predictions for the impact of specific system properties on the qualitatively behavior of the Tafel plots. A theoretical analysis of EPCET was based on the following approximate expressions for the heterogeneous PCET anodic and cathodic nonadiabatic rate constants:

$$
\begin{aligned}
k_a(\eta) &= \frac{(V^{el}S)^2}{\hbar}\sqrt{\frac{\pi}{k_B T\Lambda}}\exp\left[2\alpha^2 k_B T/F_R\right]\varrho_M \\
&\quad\times\int d\varepsilon\,[1-f(\varepsilon)]\exp\left[-\frac{(\Delta\tilde{U}+\varepsilon-e\eta+\Lambda+2\alpha\delta Rk_B T)^2}{4\Lambda k_B T}\right] \\
k_c(\eta) &= \frac{(V^{el}S)^2}{\hbar}\sqrt{\frac{\pi}{k_B T\Lambda}}\exp\left[-2\alpha\delta R+2\alpha^2 k_B T/F_R\right]\varrho_M \\
&\quad\times\int d\varepsilon f(\varepsilon)\exp\left[\frac{(-\Delta\tilde{U}-\varepsilon+e\eta+\Lambda-2\alpha\delta Rk_B T)^2}{4\Lambda k_B T}\right]
\end{aligned}
\tag{1.47}
$$

Here, $f(\varepsilon)$ is the Fermi distribution function for the electronic states in the electrode, $\varrho_M$ is the density of states at the Fermi level, $\eta$ is the overpotential defined as the difference between the applied and the formal electrode potentials, $V_{el}$ is the

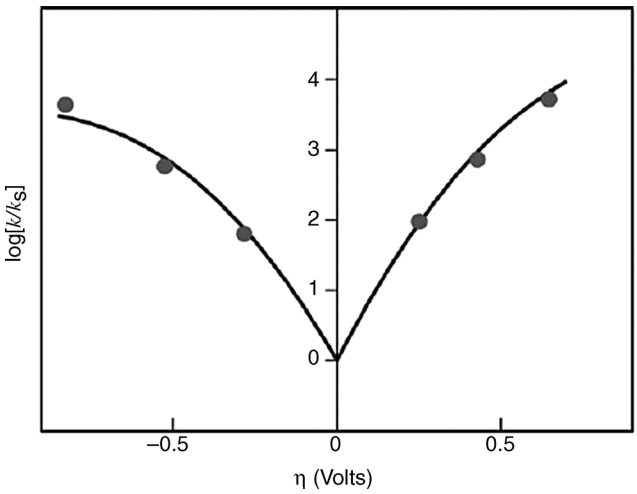


**Figure 1.23** Tafel plot of $\log[k_c/k_s]$ for $\eta < 0$ and $\log[k_a/k_s]$ for $\eta > 0$ calculated using Equation 1.1. The experimental data on the of PCET(0) in Osmium Aquo Complex generated at pH 6.0 are shown as circles [122].

electronic coupling, $\delta R$ is the difference between the equilibrium proton donor–acceptor distances for the oxidized and reduced complexes, $F_R$ is the force constant associated with the proton donor–acceptor mode, $S$ is the overlap integral between the ground reactant and the product proton vibrational wave functions, $\alpha = -\partial \ln S/\partial R$, and $\Lambda = \lambda_s + \lambda_R$ is the total reorganization energy, where $\lambda$s is the solvent reorganization energy and $\lambda_R = F_R \delta R^2/2$ is the reorganization energy of the proton donor–acceptor mode.

According the theory, the associated cathodic transfer coefficient at small overpotential $\eta$ is

$$\alpha_{PCET}(\eta) = \frac{1}{2} - \frac{\alpha \delta R k_B T}{\Lambda} + \frac{e\eta}{2\Lambda} \tag{1.48}$$

The $\pm 2\alpha\delta R k_B T$ terms in the exponentials of Equation 1.45 lead to asymmetry of the Tafel plots, and the $\alpha\delta R k_B T/\Lambda$ term leads to deviation of $\alpha_{PCET(0)}$ from one-half predicted from classic linear Tafel plot (Figure 1.23).

A study [136] treated the role of the density of electronic states $\varrho_F$ at the Fermi level of a metal in affecting the rate of nonadiabatic electron transfer. The rate constant $k_{ET}$ was calculated for the electron transfer across an alkanethiol monolayer on platinum and on gold. It was shown that the metal bands that are weakly coupled contribute much less to the rate constant than was suggested by their density of states $\varrho_F$. The authors concluded that $k_{ET}$ is approximately independent of $\varrho_F$ in two cases: (1) adiabatic electron transfer and (2) nonadiabatic electron transfer when the extra $\varrho_F$ is due to the *d* electrons. The temperature dependence of the electronic contribution to the nonadiabatic electron transfer rate constant ($k_{ET}$) at metal electrodes was discussed [137]. It was found that this contribution is proportional to the absolute

temperature $T$. The nonadiabatic rate constant for electron transfer at a semiconductor electrode was also considered. Under conditions for the maximum rate constant, the electronic contribution was estimated to be proportional to $T$, but for different reasons from those the case of metals, that is, Boltzmann statistics and transfer at the conduction band edge for the semiconductor versus Fermi–Dirac statistics and transfer at the Fermi level, which is far from the band edge, of the metal.

Molecular dynamics simulations of electron and ion transfer reactions near a smooth surface were presented [136]. The effect of the geometrical constraint of the surface and the interfacial electric field on the relevant solvation properties of both a monovalent negative ion and a neutral atom was analyzed. The quantum mechanical electron transfer between the metal surface and the ion/atom in solution was done by the MD simulation using a model Hamiltonian. The authors calculated two-dimensional free energy surfaces for ion adsorption allowing for partial charge transfer.

A generalized quantum master equation theory that governs the quantum dissipation and quantum transport was formulated in terms of hierarchically coupled equations of motion for an arbitrary electronic system in contact with electrodes under either a stationary or a nonstationary electrochemical potential bias [137]. The multiple frequency dispersion and the non-Markovian reservoir parameterization schemes were considered. The resulting hierarchical equations of motion formalism was applied to arbitrary electronic systems, including Coulomb interactions, under the influence of arbitrary time-dependent applied bias voltage and external fields. The authors claimed that the present theory provides an exact and numerically tractable tool to evaluate various transient and stationary quantum transport properties of many-electron systems, together with the involving nonperturbative dissipative dynamics.

Effects of electron correlations in a surface molecule model for the adiabatic electrochemical electron transfer reactions with allowance for the electrostatic repulsion of electrons on an effective orbital of metal was considered [138]. It was shown that taking into account the electrostatic repulsion on the effective orbital of the metal and the correlation effects leads to qualitative different forms of adiabatic free energy surfaces in some regions of values of the model's parameters. Approximate method for calculation of electron transition probability for simple outer-sphere electrochemical reactions was developed [139]. The probability of an elementary act in an outer-sphere electrochemical electron transfer reaction was calculated with arbitrary values of the parameter of reactant–electrode electron interaction for diabatic free energy surfaces of the parabolic form. The dependence of effective transmission coefficient on the Landau–Zener parameter was found. Interpolation formulas obtained allowed authors to calculate the electron transition probability using the results of quantum chemical calculation of the electronic matrix element as a function of distance.

Direct electrochemistry of redox enzymes as a tool for mechanistic studies was proposed [140]. The following analytical expression for the rate of redox processes was

$$k_{\mathrm{red/ox}} = \frac{k_{\max}}{\sqrt{4\pi\lambda/RT}} \int_{-\infty}^{\infty} \frac{\exp\left(-(1/4\lambda RT)[\lambda \pm F(E-E^0)-RTx]^2\right)}{1+\exp(x)}\,\mathrm{d}x \tag{1.49}$$

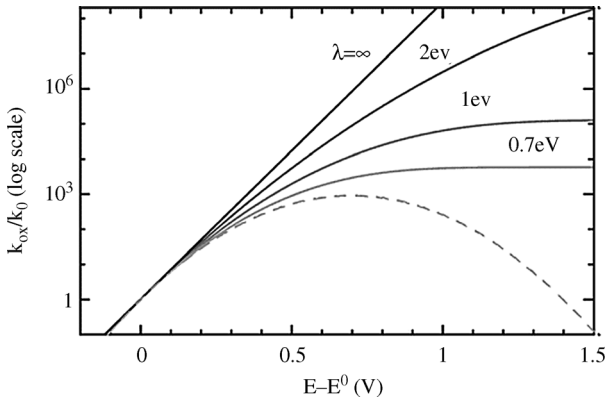


**Figure 1.24** Dependence of the rate of interfacial, oxidative ET on the electrode potential according to the BV (black) or Marcus theory of interfacial ET for different values of the reorganization energy $\lambda$ (solid gray lines). The dashed line is the traditional Marcus paraboloid with $\lambda = 0.7$ eV, showing the inverted region at high driving force. For interfacial ET, the rate levels off at a high driving force instead of decreasing [141].

where $k_{max}$ is the asymptotic value of the rate constant at large overpotential. Equation 1.49 is referred to as Marcus theory applied to interfacial ET kinetics. Dependence of the rate of interfacial, oxidative ET on the electrode potential is displayed in Figure 1.24.

## 1.3 Concerted and Multielectron Processes

In order to explain the high efficiency of many chemical and enzymatic processes, the concept of energetically favorable, concerted mechanisms is widely used.

In a concerted reaction, a substrate is simultaneously attracted by different active reagents with acid and basic groups, nucleophile and electrophile, or reducing and oxidizing agents. It may, however, be presumed that certain kinetic statistic limitation exists on realization of reactions that are accompanied by a change in the configuration of a large number of nuclei [9, 142–148]. A concerted reaction occurs as a result of the simultaneous elementary transition (taking approximately $10^{-13}$ s) of a system of independent oscillators, with the mean displacement of nuclei $\varphi_0$, from the ground state to the activated state in which this displacement exceeds for each nucleus a certain critical value ($\varphi_{cr}$). If $\varphi_{cr} > \varphi_0$ and the activation energy of the concerted process $E_{syn} > nRT$, the theory gives the following expression for the synchronization factor $\alpha_{syn}$, which is the ratio of preexponential factors synchronous and regular processes:

$$\alpha_{syn} = \frac{n}{2^{n-1}} \left( \frac{nRT}{\pi E_{syn}} \right)^{n-1/2} \tag{1.50}$$

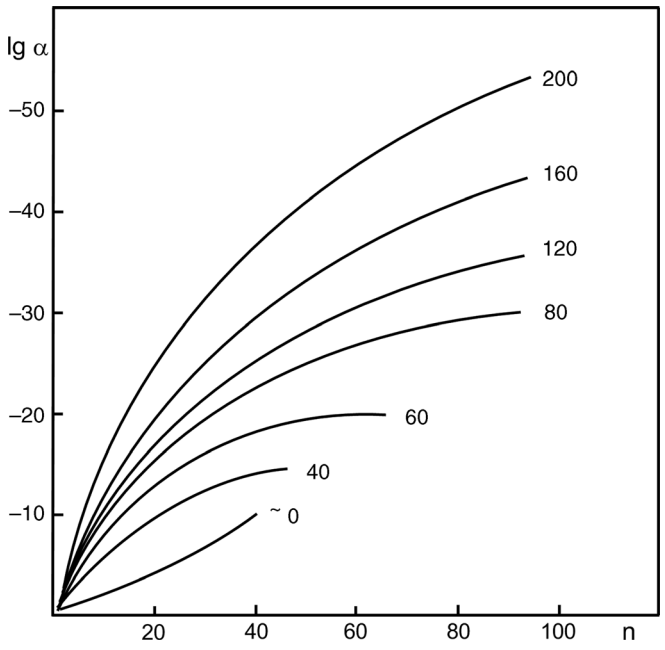


**Figure 1.25** Theoretical dependence of the synchronization factor ($f_{syn}$) on the number of degree of freedom ($n$) of nuclei involved in a concerted reaction. The curves have been constructed in accordance with Equation 1.50 [9]. Energy activation of the synchronous reaction is given in kJ/mol [156].

Analysis of Equation 1.50 provides a clear idea of the scale of the synchronization factor and dependence of this factor on the number of $n$ and the energy activation (Figure 1.25) [9, 150]. For example, at moderate energy activation 20–30 kJ/mol, the incorporation of each new nucleus into the transition state can lead to a 10-fold decrease in the rate of the process.

The model of concerted processes discussed above is only a crude approximation of the motion of a complex system of nuclei along the reaction coordinate. However, such an approximation apparently permits one to choose from among the possible reaction mechanisms.

In the case of effective concerted mechanism, the decrease in the synchronization probability ($\alpha_{syn}$) with increasing $n$ must be compensated for by an appreciable decrease in the activation energy. This consideration has led to the formulation of the principle of *optimum motion* [9, 144–147]. According to this principle, the number of nuclei whose configuration is charged in the elementary act of a chemical reaction (including electron transfer) must be sufficiently large to provide favorable energetic of the step and, at the same time, sufficiently small for the maintenance of a high value of the synchronization probability during motion along the reaction pathway to the reaction products.

There are a considerable number of reactions in which the products contain two electrons more than the starting compounds, and the consecutive several-step

one-electron transfer process proves to be energetically unfavorable. In such cases, it is presumed that two-electron process occurs in one elementary two-electron step.

Two-electron mechanism may involve the direct transport of two electrons from a mononuclear transition complex to a substrate. Such a transport may alter sharply the electrostatic states of the systems and obviously require a substantial rearrangement of the nuclear configuration of ligands and polar solvent molecules. For instance, the estimation of the synchronization factor ($\alpha$) for an octahedral complex with low molecular saturated ligands shows a very low value of $\alpha = 10^{-7}$–$10^{-8}$ and, therefore, a very low rate of reaction. The probability of two-electron processes, however, increases sharply if compensation shift of electronic cloud from bulky nonsaturated ligands to central metal atom takes place. Involvement of bi- and, especially, polynuclear transition metal complexes and metal clusters, as well as synchronous proton transfer, may essentially decrease the environment reorganization and, therefore, provide a high rate for the two- and four-electron mechanisms.

The concept of four-electron mechanism was first suggested in Ref. [151] and then developed and applied to such "heavy" enzymatic and chemical reactions as the reduction of molecular nitrogen and the water splitting under mild conditions [144, 147, 149, 151–155].

The multielectron nature of the energetically favorable processes in clusters does not evidently impose any new, additional restrictions on its rate. Within the clusters' coordination sphere, the multiorbital overlap is effective and, therefore, the resonance integral $V$ is high. The electron transfer from (or to) the orbitals of the metal to substrate orbital is accompanied by the simultaneous shift of electron clouds to the reverse direction. Such a transport may prevent significant changing of local charges and does not violate markedly the reaction complex nuclear frame. The strong delocalization electron in clusters and polynuclear complexes reduces to minimum the reorganization of the nuclear system during electron transitions and, therefore, provides low energy activation and a relatively high value for the synchronization factor.

The data presented in this chapter show that a particularly significant contribution has been recently made to the theory of electron transfer, which has formed the theoretical basis for a deeper understanding and effective planning of redox processes in dye-sensitized solar cells and other photochemical systems.

## References


1 Jortner, J. and Bixson, M. (eds.) (1999) Electron transfer: from isolated molecules to biomolecules, in *Advances in Chemical Physics*, vol. **107**, Parts 1 and 2, John Wiley & Sons, Inc., NY.

2 Marcus, R.A. (1968) *J. Phys. Chem.*, **72** (8), 891–899.

3 Marcus, R.A. (1999) Electron transfer past and future, in *Advances in Chemical Physics*, vol. **107**, Part 1 (eds. J. Jortner and M. Bixon), John Wiley & Sons, Inc., NY, pp. 1–6.

4 Hush, N.S. and Reimers, J.R. (1998) *Coordin. Chem. Rev.*, **177** (1), 37–60.

5 Marcus, R.A. (2000) *J. Electroanal. Chem.*, **483** (1), 2), 2–6.

6 Sutin, N. (1999) Electron transfer reaction in solution: a historical

perspective, in *Advances in Chemical Physics*, vol. **107**, Part 1 (eds. J. Jortner and M. Bixon), John Wiley & Sons, Inc., NY, pp. 7–33.
7 Gust, D., Moore, T.A., and Moore, A.L. (2009) *Acc. Chem. Res.*, **42** (12), 1890–1898.
8 Rutherford, A.W. and Moore, T.A. (2008) *Nature (London)*, **453** (7194), 449–453.
9 Likhtenshtein, G.I. (2003) *New Trends In Enzyme Catalysis and Mimicking Chemical Reactions*, Kluwer Academic/Plenum Publishers, Dordrecht.
10 Blankenship, R.E. (2002) *Molecular Mechanisms of Photosynthesis*, Blackwell Science, Oxford.
11 Feskov, S.V., Ivanov, A.I., and Burshtein, A.I. (2005) *J. Chem. Phys.*, **122** (12), 124509/1–124509/11.
12 Hall, D.O. and Krishna, R. (1999) *Photosynthesis*, 6th edn, Cambridge University Press, Cambridge.
13 Collings, A.F. and Critchley, C. (2005) *Artificial Photosynthesis: From Basic Biology to Industrial Application*, Wiley-VCH Verlag GmbH, Weinheim.
14 Lawlor, D. (2000) *Photosynthesis*, Kluwer Academic, Dordrecht.
15 Kenneth, K.C. (1992) *Energy Conversion (West - Engineering Series)*, PWS Pub. Co., electronic edition, revised from the 1992 edition.
16 Wurfel, P. (2009) *Physics of Solar Cells: From Basic Principles to Advanced Concepts*, 2nd edn, Wiley-VCH Verlag GmbH, Weinheim.
17 Marcus, R.A. and Sutin, N. (1985) *Biochim. Biophys. Acta*, **811** (2), 265–322.
18 Mikhailova, V.A. and Ivanov, A.I. (2007) *J. Phys. Chem. C*, **111** (11), 4445–4451.
19 Bixon, M. and Jortner, J. (1999) Electron transfer: from isolated molecules to biomolecules, in *Advances in Chemical Physics*, vol. **107**, Part 1 (eds. J. Jortner and M. Bixon), John Wiley & Sons, Inc., NY, pp. 35–202.
20 Gray, H.B. and Winkler, JR. (1996) *Annu. Rev. Biochem.*, **65**, 537–561.
21 McLendon, G., Komar-Panicucci, S., and Hatch, S. (1999) *Adv. Chem. Phys.*, **107**, 591–600.
22 Khokhlova, S.S., Mikhailova, V.A., and Ivanov, A.I. (2008) *Russ. J. Phys. Chem. A*, **82** (6), 1024–1030.
23 Lluch, J.M. (2000) *Theor. Chem. Acc.*, **103** (3–4), 231–233.
24 Wurfel, P. (2009) *Physics of Solar Cells: From Basic Principles to Advanced Concepts*, 2nd edn, Wiley-VCH Verlag GmbH, Weinheim.
25 Wenham, S.R., Green, M.A., Watt, M.E., and Corkish, R. (2007) *Applied Photovoltaics*, 2nd edn, Earthscan Publications Ltd., London.
26 Green, M.T. (2005) *Generation Photovoltaics: Advanced Solar Energy Conversion, Springer Series in Photonics*, Springer, Heidelberg.
27 Marcus, R.A. (1997) *Pure Appl. Chem.*, **69** (1), 13–29.
28 Chernick, E.T., Mi, Q., Vega, A.M., Lockar, J.V., Ratner, M., and Wasielewski, M.R. (2007) *J. Phys. Chem. B*, **111** (24), 6728–6737.
29 Kurnikov, I.V., Zusman, L.D., Kurnikova, M.G., Farid, R.S., and Beratan, D.N. (1997) *J. Am. Chem. Soc.*, **119** (24), 5690–5700.
30 Egorova, D., Thoss, M., Domcke, W., and Wang, H. (2003) *J. Chem. Phys.*, **119** (5), 2761–2773.
31 Khudyakov, I., Zharikov, A.A., and Burshtein, A.I. (2010) *J. Chem. Phys.*, **132** (1), 014104/1–014104/6.
32 Leontyev, I.V., Vener, M.V., Rostov, I.V., Basilevsky, M.V., and Newton, M.D. (2003) *J. Chem. Phys.*, **119** (15), 8024–8037.
33 Likhtenshtein, G.I., Nakatsuji, S., and Ishii, K. (2007) *Photochem. Photobiol.*, **83** (4), 871–881.
34 Likhtenshtein, G.I., Pines, D., Pines, E., and Khutorsky, V. (2009) *Appl. Magn. Reson.*, **35** (3), 459–472.
35 Gamov, C.A. (1926) *Quanum Theo. Atoms Phys.*, **51** (2), 204–212.
36 Marcus, R.A. (1956) *J. Chem. Phys.*, **24**, 966–978.
37 Hush, N.S. (1958) *J. Chem. Phys.*, **28** (5), 962–972.
38 Fermi, E. (1950) *Nuclear Physics*, University of Chicago Press, Chicago.
39 Landau, L. (1932) *Phyz. Soviet Union*, **2** (1), 46–51.

**40** Zener, C. (1933) *Proc. Royal. Soc. London*, **A140**, 660–668.

**41** Levich, V.G. and Dogonadze, R. (1960) *Dokl. Acad. Nauk.*, **133** (1), 159–161.

**42** Levich, V.G., Dogonadze, R., German, E., Kuznetsov, A.M., and Kharkats, Y.I. (1970) *Electrochem. Acta*, **15** (2), 353–368.

**43** German, E.D. and Kuznetsov, A.M. (1994) *J. Phys. Chem.*, **98** (24), 6120–6127.

**44** Efrima, S. and Bixon, M. (1974) *Chem. Phys. Lett.*, **25** (1), 34–37.

**45** Nitzan, A., Jortner, J., and Rentzepis, P.M. (1972) *Proc. Royal Soc. London*, **A327** (2), 367–391.

**46** Neil, R., Kestner, N.R., Logan, J., and Jortner, J. (1974) *J. Phys. Chem.*, **78** (21), 2148–2166.

**47** Hopfield, J.J. (1974) *Proc. Natl. Acad. Sci. USA*, **71** (9), 3640–3644.

**48** Grigorov, L.N. and Chernavsky, D.S. (1972) *Biofizika*, **17** (2), 195–202.

**49** Costentin, C. (2008) *Chem. Rev.*, **108** (7), 2145–2179.

**50** Burshtein, A.I. (2000) United theory of photochemical charge separation, in *Advances in Chemical Physics*, vol. **114** (eds I. Prigogine and A. Rice), John Wiley & Sons, Inc., pp. 419–587.

**51** Benjamin, I. and Pollak, E. (1996) *J. Chem. Phys.*, **105** (20), 9093–9910.

**52** Kurnikov, I.V., Zusman, L.D., Kurnikova, M.G., Farid, R.S., and Beratan, D.N. (1997) *J. Am. Chem. Soc.*, **119** (24), 5690–5700.

**53** Freed, K.F. (2003) *J. Phys. Chem. B*, **107** (38), 10341–10343; Egorova, D., Thoss, M., Domcke, W., and Wang, H. (2003) *J. Chem. Phys.*, **119** (5), 2761–2773.

**54** Kuznetsov, A.M., Sokolov, V.V., and Ulstrup, J. (2001) *J. Electroanal. Chem.*, **502** (1–2), 36–46.

**55** Zhou, H.-X. and Szabo, A. (1995) *J. Chem. Phys.*, **103** (9), 3481–3494; Zhao, Y. and Liang, W.Z., *Phys. Rev. A Atom. Mol. Opt. Phys.*, **74** (3 Pt A), 032706/1–032706/5.

**56** Wu, Q. and Van Voorhis, T. (2006) *J. Chem. Phys.*, **125** (16), 164105/1–164105/9.

**57** Migliore, A., Corni, S.I., Felice, R., and Molinari, E. (2006) *J. Chem. Phys.*, **124** (6), 064501/1–064501/16.

**58** Zhu, C. and Nakamura, H. (2001) *Adv. Chem. Phys.*, **117**, 127–166.

**59** Zhao, Y. and Liang, W. (2006) *Phys. Rev. A Atom. Mol. Opt. Phys.*, **74** (3 Pt A), 032706/1–032706/5.

**60** Zhao, Y. and Nakamura, H. (2006) *J. Theor. Comput. Chem.*, **5** (Special Issue), 299–306.

**61** Aubry, S. (2007) *J. Phys. Condens. Matter*, **19** (25), 255204/1–255204/30.

**62** Dougherty, R.C. (1997) *J. Chem. Phys.*, **106** (7), 2621–2626.

**63** Newton, M.D. (2004) in *Comprehensive Coordination Chemistry II*, vol. **2**, pp. 573–587.

**64** Finklea, H.O. (2007) *Encycloped. Electrochem.*, **11**, 623–650.

**65** Newton, M.D. (1999) Control of electron transfer kinetics: models for medium reorganization and donor–acceptor coupling, in *Advances in Chemical Physics*, vol. **107**, Part 1 (eds. J. Jortner and M. Bixon), John Wiley & Sons, Inc., NY, pp. 303–376.

**66** VandeVondele, J., Ayala, R., Sulpizi, M., and Sprik, M. (2007) *J. Electroanal. Chem.*, **607** (1–2), 113–120.

**67** Wu, Q. and Van Voorhis, T. (2006) *J. Phys. Chem. A*, **110** (29), 9212–9218.

**68** Berlin, Y.A., Grozema, F.C., Siebbeles, L.D.A., and Ratner, M.A. (2008) *J. Phys. Chem. C*, **112** (29), 10988–11000.

**69** Jang, S. and Newton, M.D. (2005) *J. Chem. Phys.*, **122** (2), 024501/1–024501/15.

**70** Basilevsky, M.V., Rostov, I.V., and Newton, M.D. (1998) *J. Electroanal. Chem.*, **450** (1), 69–82.

**71** Fletcher, S. (2007) *J. Solid State Electrochem.*, **11** (5), 965–969.

**72** Fletcher, S. (2008) *J. Solid State Electrochem.*, **12** (4), 765–770.

**73** Liang, K.K., Mebel, A.M., Lin, S.H., Hayashi, M., Selzle, H.L., Schlag, E.W., and Tachiya, M. (2003) *Phys. Chem. Chem. Phys.*, **5** (20), 4656–4665.

**74** Rasaiah, J.C. and Zhu, J. (2008) *J. Chem. Phys.*, **129** (21), 214503/1–214503/5.

**75** Chen, Y., Xu, R.-X., Ke, H.-W., and Yan, Y.-J. (2007) *Chin. J. Chem. Phys.*, **20** (4), 438–444.

**76** de la Lande, A. and Salahub, D.R. (2010) *J. Mol. Struct. Theochem*, **943** (1–3), 115–120.

**77** Kharkatz, Y.I. (1976) *Electrokhimia*, **12**, 592–595.

**78** Miyashita, O. and Go, N. (2000) *J. Phys. Chem.*, **104**, 7516–7521.

**79** Georgievskii, Y., Hsu, C., and Marcus, R.A. (1999) *J. Chem. Phys.*, **110** (11), 5307–5317.

**80** Zusman, L.D. (1980) *Chem. Phys.*, **49** (2), 295–304.

**81** Zusman, L.D. (1983) *Chem. Phys.*, **80** (1–2), 29–43.

**82** Zusman, L.D. (1991) *Electrochim. Acta*, **36** (3–4), 395–399.

**83** Zhang, M.-L., Zhang, S., and Pollak, E. (2003) *J. Chem. Phys.*, **119** (22), 11864–11877.

**84** Shi, Q., Chen, L., Nan, G., Xu, R., and Yan, Y. (2009) *J. Chem. Phys.*, **130** (16), 164518/1–164518/7.

**85** Tanaka, M. and Tanimura, Y. (2009) *J. Phys. Soc. Jpn.*, **78** (7), 073802/1–073802/4.

**86** Zhang, M.-L., Zhang, S., and Pollak, E. (2003) *J. Chem. Phys.*, **119** (22), 11864–11877.

**87** Schröder, M., Schreiber, M., and Kleinekathöfer, U. (2007) *J. Chem. Phys.*, **126**, 114102.

**88** Casado-Pascual, J., Goychuk, I., Morillo, M., and Hanggi, P. (2002) *Chem. Phys. Lett.*, **3603** (4), 333–339.

**89** Casado-Pascual, J., Morillo, M., Goychuk, I., and Hanggi, P. (2003) *J. Chem. Phys.*, **118** (1), 291–303.

**90** Kuznetsov, A.M. and Ulstrup, J. (2001) *Electrochim. Acta*, **46** (20–21), 3325–3333.

**91** Likhtenshtein, G.I. (1996) *J. Phochem. Photobiol. A Chem.*, **96** (1), 79.

**92** Zhou, H.-X. and Szabo, A. (1995) *J. Chem. Phys.*, **103** (9), 3481–3494.

**93** Banerjee, S. and Gangopadhyay, G. (2007) *J. Chem. Phys.*, **126** (3), 034102/1–034102/14.

**94** Beratan, D.N., Onuchic, J.N., Betts, J.N., Bowler, B.E., and Gray, G.H. (1990) *J. Am. Chem. Soc.*, **112** (34), 7915–7921.

**95** Cook, W.R., Coalson, R.D., and Evans, D.G. (2009) *J. Phys. Chem. B*, **113** (33), 11437–11447; Marcus, R.A. (1997) *Pure Appl. Chem.*, **69** (1), 13–29.

**96** Stuchebrukov, A.A. and Marcus, R.A. (1995) *J. Phys. Chem.*, **99** (19), 7581–7590.

**97** Scourotis, S.S. and Beratan, D.N. (1999) Theories of structure–function relationships for bridge-mediated electron transfer reaction, in *Advances in Chemical Physics*, vol. **107**, Part 1 (eds J. Jortner and M. Bixon), John Wiley & Sons, Inc., NY, pp. 377–452.

**98** Balabin, I.A. and Onuchic, J.N. (2000) *Science*, **290**, 114–117.

**99** Kosloff, R. and Ratner, M.A. (1990) *Isr. J. Chem.*, **30** (1–2), 45–58.

**100** Likhtenshtein, G.I. (2008) *Pure and Appl. Chem.*, **80** (10), 2125–2139.

**101** Zamaraev, K.I., Molin, Y.N., and Salikhov, K.M. (1981) Spin exchange, in *Theory and Physicochemical Application*, Springer, Heidelberg.

**102** Ermolaev, V.L., Bodunov, E.N., Sveshnikova, E.B., and Shakhverdov, T.A. (1977) *Radiationless Transfer of Electronic Excitation Energy*, Nauka, Leningrad.

**103** Chong, S.-H. and Hirata, F. (1995) *J. Mol. Liq.*, **65–66**, 345–348.

**104** Siddarth, P. and Marcus, R.A. (1993) *J. Phys. Chem.*, **97** (11), 2400–2405.

**105** Siddarth, P. and Marcus, R.A. (1993) *J. Phys. Chem.*, **97** (23), 6111–6114.

**106** Siddarth, P. and Marcus, R.A. (1993) *J. Phys. Chem.*, **97** (50), 13078–13082.

**107** Tanimura, Y., Leite, V.B.P., and Onuchic, J.N. (2002) *J. Chem. Phys.*, **117** (5), 2172–2179.

**108** Okada, A., Chernyak, V., and Mukamel, S.J. (1998) *Phys. Chem. A*, **102** (8), 1241–1251.

**109** Aubry, S. and Kopidakis, G. (2005) *J. Biol. Phys.*, **31** (3–4), 375–402.

**110** Buchachenko, A.L. and Berdinsky, V.L. (2002) *Chem. Rev.*, **102** (3), 603–612.

**111** Buchachenko, A.L. and Kuznetsov, D.A. (2006) *Mol. Biol.*, **40** (1), 9–15.

**112** Okamura, M.Y. and Feher, G. (1986) *Proc. Natl. Acad. Sci. US A*, **83** (21), 8152–8156.

**113** Cukier, R.I. (2002) *J. Phys. Chem. B*, **106** (7), 1746–1757.

**114** Cukier, R.I. (1996) *J. Phys. Chem.*, **100** (38), 15428–15443.

**115** Cukier, R.I. and Nocera, D.G. (1998) *Annu. Rev. Phys. Chem.*, **49**, 337–369.

**116** Chakraborty, A. and Hammes-Schiffer, S. (2008) *J. Chem. Phys.*, **129** (20), 204101/1–204101/16.

**117** Hammes-Schiffer, S., and Soudackov, A.V. (2008) *J. Phys. Chem. B*, **112** (45), 14108–14123.

**118** Venkataraman, C., Soudackov, A.V., and Hammes-Schiffer, S. (2008) *J. Phys. Chem. C*, **112** (32), 12386–12397.

**119** Hatcher, E., Soudackov, A., and Hammes-Schiffer, S. (2005) *J. Phys. Chem. B*, **109** (39), 18565–18574.

**120** Hammes-Schiffer, S. (2001) *Acc. Chem. Res.*, **34** (4), 273–281.

**121** Moore, D.B. and Martinez, T.J. (2000) *J. Phys. Chem. A*, **104** (11), 2525–2531.

**122** Ludlow, M.K., Soudackov, A.V., and Hammes-Schiffer, S. (2010) *J. Am. Chem. Soc.*, **132** (4), 1234–1235.

**123** Venkataraman, C., Soudackov, A.V., and Hammes-Schiffer, S. (2010) *J. Phys. Chem. C*, **114** (1), 487–496.

**124** Kuznetsov, A.M. and Medvedev, I.G. (2008) *Russ. J. Electrochem.*, **44** (2), 167–186.

**125** Fermi, E. (1926) *Rend. Lincei*, **3**, 145–149.

**126** Dirac, P.A.M. (1926) *Proc. R. Soc. Series A*, **112**, 661–677.

**127** Dirac, P.A.M. (1967) *Principles of Quantum Mechanics* (revised 4th ed.), Oxford University Press, London, pp. 210–211.

**128** Sommerfeld, A. (1927) *Naturwissenschaften*, **15** (41), 824–832.

**129** Kittel, C. and Kroemer, H. (1980) *Thermal Physics*, 2nd edn, W.H. Freeman, San Francisco, p. 357.

**130** Zusman, L.D. (1992) *Chem. Phys. Lett.*, **200** (4), 379–381.

**131** Bramwell, S.T., Giblin, S.R., Calder, S., Aldus, R., Prabhakaran, D., and Fennell, T. (2009) *Nature*, **461** (7266), 956–960.

**132** Ryo, A., Masahiro, K., and Fumio, H. (1999) *Chem. Phys. Lett.*, **305** (3), 251–257.

**133** Sakata, T. (1996) *Bull. Soc. Chem. Jpn.*, **69** (9), 2435–2446.

**134** Gosavi, S. and Marcus, R.A. (2000) *J. Phys. Chem. B*, **104** (9), 2067–2072.

**135** Gosavi, S., Gao, Y.Q., and Marcus, R.A. (2001) *J. Electroanal. Chem.*, **500** (1–2), 71–77.

**136** Hartnig, C. and Koper, M.T.M. (2003) *J. Am. Chem. Soc.*, **125** (32), 9840–9845.

**137** Jin, J., Zheng, X., and Yan, Y. (2008) *J. Chem. Phys.*, **128** (23), 234703/1–234703/15.

**138** Kokkanen, A.A., Kuznetsov, A.M., and Medvedev, I.G. (2007) *Russ. J. Electrochem.*, **43** (9), 1033–1046.

**139** Kokkanen, A.A., Kuznetsov, A.M., and Medvedev, I.G. (2008) *Russ. J. Electrochem.*, **44** (4), 397–407.

**140** Leger, C. and Bertrand, P. (2008) *Chem. Rev.*, **108** (7), 2379–2483.

**141** Chidsey, C.E.D. (1991) *Science*, **251** (4996), 919–922.

**142** Bordwell, F.G. (1970) *Acc. Chem. Res.*, **3**, 281–290.

**143** Likhtenshtein, G.I. (1974) *Spin Labeling Method in Molecular Biology*, Nauka, Moscow.

**144** Likhtenshtein, G.I. (1976) *Spin Labeling Method in Molecular Biology*, Wiley Interscience, NY.

**145** Likhtenshtein, G.I. (1977) *Kinet. Catal.*, **28**, 878–882.

**146** Likhtenshtein, G.I. (1977) *Kinet. Catal.*, **28**, 1255–1260.

**147** Likhtenshtein, G.I. (1988) *Chemical Physics of Redox Metalloenzymes*, Springer, Heidelberg.

**148** Bernasconi, C.F. (1992) *Acc. Chem. Res.*, **25**, 9–16.

**149** Denisov, E.T., Sarkisov, O.M., and Likhtenshtein, G.I. (2003) *Chemical Kinetics: Fundamentals and Recent Developments*, Elsevier Science.

**150** Alexandrov, I.V. (1976) *Theor. Exper. Khim*, **12**, 299–306.

**151** Likhtenshtein, G.I. and Shilov, A.E. (1970) *Zhurnal Fiz. Khem.*, **44**, 849–856; Semenov, N.N., Shilov, A.E., and Likhtenshtein (1975) *Dokl. Acad. Nauk SSSR*, **221**, 1374–1377.

**152** Likhtenshtein, G.I., Kotel'nikov, A.I., Kulikov, A.V., Syrtsova, L.A., Bogatyrenko, V.R., Mel'nikov, A.I., Frolov, E.N., and Berg, A.J. (1979) *Int. J. Quantum Chem.*, **16** (3), 419–435.

**153** Likhtenshtein, G.I. (1988) *J. Mol. Catal.*, **48**, 129–138.

**154** Likhtenshtein, G.I. (1990) *Pure Appl. Chem.*, **62**, 281–288.

**155** Likhtenshtein, G.I. (1985) in (ed. Y.A. Ovchinnikov), Proceedings of the 16th FEBS Congress (1985), A, p. 9.